

Accuracy and convergence of velocity formulations for water waves in the framework of Boussinesq theory

By P. A. MADSEN¹ AND Y. AGNON²

¹Department of Mechanical Engineering, Technical University of Denmark,
DK 2800 Kgs. Lyngby, Denmark

²Civil Engineering, Technion, Haifa 32000, Israel

(Received 15 May 2002 and in revised form 30 September 2002)

The objective of this paper is to discuss and analyse the accuracy of various velocity formulations for water waves in the framework of Boussinesq theory. To simplify the discussion, we consider the linearized wave problem confined between the still-water datum and a horizontal sea bottom. First, the problem is further simplified by ignoring boundary conditions at the surface. This reduces the problem to finding truncated series solutions to the Laplace equation with a kinematic condition at the sea bed. The convergence and accuracy of the resulting expressions is analysed in comparison with the target cosh- and sinh-functions from linear wave theory. First, we consider series expansions in terms of the horizontal velocity variable at an arbitrary z -level, which can be varied from the sea bottom to the still-water datum. Second, we consider the classical possibility of expanding in terms of the depth-averaged velocity. Third, we analyse the use of a horizontal pseudo-velocity determined by interpolation between velocities at two arbitrary z -levels. Fourth, we investigate three different formulations based on two expansion variables, being the horizontal and vertical velocity variables at an arbitrary z -level. This is shown to have a remarkable influence on the convergence and to improve accuracy considerably. Fifth, we derive and analyse a new formulation which doubles the power of the vertical coordinate without increasing the order of the horizontal derivatives. Finally, we involve the kinematic and dynamic boundary conditions at the free surface and discuss the linear dispersion relation and a spectral solution for steady nonlinear waves.

1. Introduction

In its classical form, Boussinesq wave theory represents a shallow-water approximation to the fully dispersive and nonlinear water wave problem, and the equations incorporate a balance between lowest-order dispersion and lowest-order nonlinearity (see e.g. Boussinesq 1872; Mei & Méhauté 1966; Peregrine 1967; Madsen & Mei 1969). The original use of the Boussinesq equations concentrated on the propagation of weakly nonlinear solitary waves (e.g. Madsen & Mei 1969), but in the late 1970's, use of the equations started to become popular in coastal engineering and the focus shifted towards regular cnoidal waves and irregular waves. With this shift of interest the underlying limitations in linear dispersion and nonlinearity for shorter waves became of concern.

The accuracy of linear dispersion and the possibility of improving it in the framework of Boussinesq theory has received considerable attention (see e.g. Benjamin, Bona & Mahony 1972; Dingemans 1973; Whitham 1974; Witting 1984; Madsen, Murray & Sørensen 1991; Nwogu 1993; Madsen & Schäffer 1998). Other formulations (e.g. Serre 1953; Su & Gardner 1969; Wei *et al.* 1995; Madsen & Schäffer 1998; Agnon, Madsen & Schäffer 1999; Wu 1999; Gobbi, Kirby & Wei 2000; Wu 2001) incorporate so-called ‘full nonlinearity’, which means that they include all nonlinear terms up to the retained order of dispersion, with the objective of improving nonlinear properties such as amplitude dispersion and wave–wave interaction. Of these attempts, the method presented by Agnon *et al.* (1999) provides the most direct way of achieving the same accuracy in nonlinear properties as in linear properties. The procedure is based on an exact formulation of the boundary conditions at the free surface and at the sea bottom combined with an approximate solution to the Laplace equation given in terms of truncated series expansions from the still-water datum. As a result, their equations provide accurate linear and nonlinear properties for wavenumbers times the water depth, kh , up to 6.

Having achieved a significant improvement in linear and nonlinear wave properties as in the various papers listed above, one might expect that the underlying velocity fields are of similar quality. This is, however, not necessarily the case. Boussinesq formulations are generally based on a polynomial approximation of the vertical variation of the velocity field, but surprisingly few papers (e.g. Wei *et al.* 1995; Gobbi *et al.* 2000; and Kennedy, Kirby & Gobbi 2002) have actually analysed the accuracy of these approximations. Of these, the profile provided by Gobbi *et al.* (2000) is by far the most accurate and it has been shown to be applicable for linear waves up to $kh \approx 5$, while most other Boussinesq profiles become hopelessly inaccurate for $kh \approx 1.5$ or less.

In the present work, we discuss and analyse the accuracy of various velocity formulations in the framework of Boussinesq theory. In order to focus on the quality of the polynomial approximations, we simplify the problem to linear waves on a constant depth. Furthermore, the bulk of the discussion does not consider the imbedded linear dispersion relation, which means ignoring the linearized kinematic and dynamic surface boundary conditions. What remains is the problem of finding accurate truncated series solutions to the Laplace equation with the kinematic condition at a horizontal sea bed. Most formulations are investigated in a first-order form (with third-order derivatives), a second-order form (with fifth-order derivatives) and in a fourth-order form (with ninth-order derivatives). In §2, we define the problem and summarize the exact infinite series solution of Madsen, Bingham & Liu (2002*a*) and Madsen, Bingham & Schäffer (2002*b*), which contains most other classical velocity formulations as subsets. In §3, we discuss many of the classical formulations e.g. Peregrine (1967), Nwogu (1993) and Gobbi *et al.* (2000). All of these are expanded in terms of a horizontal velocity variable defined at the still-water level, the sea bottom, the mid-depth or depth-averaged. We demonstrate that most of these formulations are restricted by a finite convergence radius. We show that in contrast to these methods, the recent formulations by Agnon *et al.* (1999) and Madsen *et al.* (2002*a, b*) have unlimited convergence radius, which makes it possible to achieve higher accuracy. We discuss and analyse three different methods from Madsen *et al.* (2002*b*) in §4, with applicability up to $kh \approx 5$, 6 and 12, respectively. In §5, we derive and analyse a new velocity formulation which provides further improvement of accuracy and applicability. In §6, we involve the linearized kinematic and dynamic boundary conditions at the free surface and discuss the quality of the

imbedded linear dispersion relation. In §7, we involve the fully nonlinear surface boundary conditions and discuss the accuracy of the velocity and pressure profiles for the case of strongly nonlinear steady waves. A summary and conclusions are given in §8.

2. The governing equations and an exact infinite series solution

The Laplace equation with appropriate boundary conditions governs the irrotational flow of an incompressible inviscid fluid bounded by the sea bed and a free surface. We simplify the fully nonlinear water wave problem on an uneven bottom to a linear problem on a constant depth. A further simplification is achieved by initially ignoring the kinematic and dynamic boundary conditions at the free surface in order to make the analysis independent of the linear dispersion relation. A Cartesian coordinate system is adopted with the x -axis and y -axis located on the still-water plane and with the z -axis pointing vertically upwards.

2.1. An infinite series solution of the Laplace equation on a constant depth

The starting point for the formulation is the Laplace equation

$$\Phi_{zz} + \nabla^2 \Phi = 0, \quad (1)$$

with the kinematic boundary condition at the horizontal sea bed,

$$\Phi_z = 0, \quad z = -h. \quad (2)$$

Here Φ is the velocity potential which is related to the velocity components through

$$\mathbf{u} \equiv \nabla \Phi, \quad w \equiv \Phi_z, \quad \nabla \equiv \left(\frac{\partial}{\partial x}, \frac{\partial}{\partial y} \right), \quad (3)$$

and ∇ is the two-dimensional gradient operator.

Recently, Madsen *et al.* (2002a, b) derived an exact solution to the Laplace equation (1) expressed in terms of

$$\mathbf{u}(x, y, z, t) = \cos((z - \hat{z})\nabla)\hat{\mathbf{u}} + \sin((z - \hat{z})\nabla)\hat{w}, \quad (4a)$$

$$w(x, y, z, t) = \cos((z - \hat{z})\nabla)\hat{w} - \sin((z - \hat{z})\nabla)\hat{\mathbf{u}}, \quad (4b)$$

where $\hat{\mathbf{u}}$, \hat{w} are the velocity components at an arbitrary level $z = \hat{z}$, and where \hat{z} is assumed to be a constant fraction (σ) of the still-water depth (h). The cos- and sin-operators are infinite Taylor series operators defined by

$$\cos(\lambda\nabla) \equiv \sum_{n=0}^{\infty} (-1)^n \frac{\lambda^{2n}}{(2n)!} \nabla^{2n}, \quad \sin(\lambda\nabla) \equiv \sum_{n=0}^{\infty} (-1)^n \frac{\lambda^{2n+1}}{(2n+1)!} \nabla^{2n+1}, \quad (5)$$

with λ being the expansion coordinate of the Taylor series. We emphasize that throughout this paper the interpretation of the powers of ∇ depends on whether this operator is acting on a scalar or a vector and in this context the following set of rules should be obeyed:

$$\begin{aligned} \nabla^{2n}\hat{\mathbf{u}} &\equiv \nabla(\nabla^{2n-2}(\nabla \cdot \hat{\mathbf{u}})), & \nabla^{2n+1}\hat{\mathbf{u}} &\equiv \nabla^{2n}(\nabla \cdot \hat{\mathbf{u}}), \\ \nabla^{2n}\hat{w} &\equiv \nabla^{2n}\hat{w}, & \nabla^{2n+1}\hat{w} &\equiv \nabla(\nabla^{2n}\hat{w}). \end{aligned}$$

The next step is to invoke the kinematic sea bed condition (2), and after inserting (4a, b) we obtain

$$\cos((h + \hat{z})\nabla)\hat{w} + \sin((h + \hat{z})\nabla)\hat{\mathbf{u}} = 0, \quad (6)$$

which defines an implicit relation between \hat{u} and \hat{w} .

Assuming a constant depth makes it easy to solve (6) to obtain the following explicit expression for \hat{w} in terms of \hat{u} ,

$$\hat{w} = -\tan((h + \hat{z})\nabla)\hat{u}. \tag{7}$$

This involves the tan-operator, which is the infinite Taylor series operator defined by the classical power series expressions for this function.

By inserting (7) in (4a, b), it is now possible to eliminate \hat{w} from the formulation of the velocity field, and we obtain

$$u(x, y, z, t) = \cos((z - \hat{z})\nabla)\hat{u} - \sin((z - \hat{z})\nabla) \tan((h + \hat{z})\nabla)\hat{u}, \tag{8a}$$

$$w(x, y, z, t) = -\cos((z - \hat{z})\nabla) \tan((h + \hat{z})\nabla)\hat{u} - \sin((z - \hat{z})\nabla)\hat{u}. \tag{8b}$$

We have now derived two alternative exact solutions to the Laplace equation: one option is (4a, b) and (6) expressed in terms of two velocity variables; the other is (8a, b) expressed in terms of a single velocity variable. On the basis of either of these expressions it is possible to recover exact linear wave theory (see §2.2). On the other hand, differences appear when truncated polynomial expansions are considered: in §3 we demonstrate that there is a penalty for applying (8a, b) due to the presence of the tan-operator. A polynomial expansion of this operator is known to have a limited convergence radius, and this limitation can only be removed if the operator is approximated by a fraction of polynomials (see §4).

2.2. Recovering Stokes linear theory

On the basis of the general infinite series expressions (4a, b) and (8a, b), we can recover Stokes linear theory for small-amplitude waves. To do this, we look for harmonic solutions of the form

$$\hat{u}(x, t) = B_1 e^{i\theta}, \quad \hat{w}(x, t) = iC_1 e^{i\theta}, \tag{9a, b}$$

where $\theta = \omega t - kx$, k is the wavenumber, ω the cyclic frequency and i the imaginary unit. Hence in Fourier space we have $\nabla = -ik$, and according to (4a, b) and (6) this leads to

$$u(x, z, t) = (\cosh(k(z - \hat{z}))B_1 + \sinh(k(z - \hat{z}))C_1)e^{i\theta}, \tag{10a}$$

$$w(x, z, t) = (\sinh(k(z - \hat{z}))B_1 + \cosh(k(z - \hat{z}))C_1)ie^{i\theta}, \tag{10b}$$

and

$$\cosh(k(h + \hat{z}))C_1 - \sinh(k(h + \hat{z}))B_1 = 0. \tag{11}$$

We insert (11) in (10a, b) and obtain

$$\frac{u(x, z, t)}{\hat{u}} = \frac{\cosh(k(z + h))}{\cosh(k(\hat{z} + h))}, \quad \frac{w(x, z, t)}{i\hat{u}} = \frac{\sinh(k(z + h))}{\cosh(k(\hat{z} + h))}, \tag{12a, b}$$

which can also be obtained directly from (8a, b). This defines the vertical variation of the velocity field in terms of \hat{u} and the variation is in agreement with Stokes linear theory.

For later use, we may determine the linearized depth-averaged velocity

$$U(x, t) \equiv \frac{1}{h} \int_{-h}^0 u(x, z, t) dz, \tag{13}$$

and express the velocity field in terms of this variable. The combination of (12a, b) and (13) yields

$$\frac{u(x, z, t)}{U} = \frac{kh \cosh(k(z+h))}{\sinh(kh)}, \quad \frac{w(x, z, t)}{iU} = \frac{kh \sinh(k(z+h))}{\sinh(kh)}. \quad (14a, b)$$

Finally, we note that if we continue the analysis and combine (12a, b) with the linearized kinematic and dynamic surface conditions at $z=0$ i.e.

$$\frac{\partial \mathbf{u}_0}{\partial t} + g \nabla \eta = 0, \quad \frac{\partial \eta}{\partial t} - w_0 = 0, \quad (15a, b)$$

we recover the exact linear dispersion relation and the velocity expressions

$$u(x, z, t) = a\omega \frac{\cosh k(z+h)}{\sinh(kh)} e^{i\theta}, \quad w(x, z, t) = a\omega \frac{\sinh k(z+h)}{\sinh(kh)} i e^{i\theta}, \quad (16a, b)$$

where a is the wave amplitude.

3. Truncated series solutions in terms of a horizontal velocity variable

Boussinesq-type expressions for the velocity field can be derived by truncating the infinite series expansions for the cos-, sin- and tan-operators. In this section, we consider expressions in terms of a horizontal velocity variable and use (8a, b) as a starting point for the derivations. At lowest order and at the next order this will recover most of the Boussinesq profiles known from the literature, and in addition a few high-order profiles will be discussed.

3.1. Analysis of profiles expressed in terms of \hat{u}

On the basis of (8a, b), we can easily derive truncated series expansions to any order, which will result in expressions of the form

$$\mathbf{u}(x, y, z, t) = \sum_{n=0}^N \alpha_{2n} \nabla^{2n} \hat{\mathbf{u}}, \quad w(x, y, z, t) = \sum_{n=0}^N \beta_{2n+1} \nabla^{2n+1} \hat{\mathbf{u}}. \quad (17a, b)$$

We emphasize that in (17a, b) the order of derivatives kept in w is always one higher than the order kept in u , in contrast to traditional Boussinesq formulations, where it is the opposite. The reason is that traditional Boussinesq formulations start from a truncated series expansion of the velocity potential, giving expressions which exactly satisfy zero vorticity but only approximately satisfy local continuity. By keeping the extra derivatives in w in (17a, b), we always exactly satisfy local continuity but only approximately satisfy zero vorticity. The expansion which we have chosen is in line with linear shallow-water-wave theory and, for higher wavenumbers, it is somewhat more accurate than the traditional expansion.

In the following we specify the solution containing up to $O(\nabla^5)$ terms, i.e. we use $N=2$ in (17a, b) with the parameters determined from an expansion of (8a, b), which yields

$$\alpha_0 \equiv 1, \quad \alpha_2 \equiv -\frac{1}{2}(z - \hat{z})^2 - (h + \hat{z})(z - \hat{z}), \quad (18a, b)$$

$$\alpha_4 \equiv \frac{1}{24}(z - \hat{z})^4 + \frac{(h + \hat{z})}{6}(z - \hat{z})^3 - \frac{(h + \hat{z})^3}{3}(z - \hat{z}), \quad (18c)$$

$$\beta_1 \equiv -(z+h), \quad \beta_3 \equiv \frac{1}{6}(z-\hat{z})^3 + \frac{(h+\hat{z})}{2}(z-\hat{z})^2 - \frac{(h+\hat{z})^3}{3}, \quad (18d, e)$$

$$\beta_5 \equiv -\frac{1}{120}(z-\hat{z})^5 - \frac{(h+\hat{z})}{24}(z-\hat{z})^4 + \frac{(h+\hat{z})^3}{6}(z-\hat{z})^2 - \frac{2}{15}(h+\hat{z})^5. \quad (18f)$$

Note that in Fourier space, (17a, b) and (18a–f) and more generally (8a, b), agree with a Taylor series expansion in kh of the target solution (12a, b).

Several classical profiles known from the literature appear as subsets of (17a, b) and (18a–f) with various choices of $\hat{z} \equiv \sigma h$: Peregrine (1967) considered lower-order formulations in terms of the surface velocity (i.e. $\sigma = 0, N = 1$), while Mei & LeMéhauté (1966), Madsen & Mei (1969) and Mei (1983) focused on expansions in terms of the bottom velocity (i.e. $\sigma = -1, N = 1$). Nwogu (1993) was the first to use an arbitrary velocity datum in a lower-order formulation ($N = 1$), and he considered the values $\sigma = -0.5528$ (leading to Padé (2,2) dispersion characteristics) and $\sigma = -0.5310$ (optimizing dispersion up to $kh = 3$). The same values of σ were used by Wei *et al.* (1995), while Chen & Liu (1995) preferred $\sigma = -0.5215$ (optimizing dispersion and shoaling). These classical lower-order profiles have been summarized in Dingemans (1997, Chap. 5.11.3), but while the original papers included only the $\alpha_0, \alpha_2, \beta_1$ terms from (18a, b, d), Dingemans included the β_3 term from (18e), which leads to a considerable improvement in the accuracy of the vertical velocity. Recently, Madsen & Schäffer (1998, Chap. 5), extended Nwogu's approach to the next order ($N = 2$) and in this process they gave expressions for the horizontal velocity including the $\alpha_0, \alpha_2, \alpha_4$ terms from (18a–f). For this case, they recommended using the value $\sigma = -0.6249$ which was determined by optimizing linear dispersion over the range from $kh = 0$ to 6. Also Dingemans (1997, Chap. 5.11.5) provided a higher-order extension of Nwogu's equations, but unfortunately a number of typographical errors appear in his differential equations as well as in his velocity profile: As an example the constant-depth version of his equation 5.493 agrees neither with his equation 5.462 nor with the α_2, α_4 terms from (18).

3.1.1. Accuracy of velocity profiles

To quantify the accuracy of the vertical variation of the velocity components, we introduce the measures

$$F_u(\sigma, kh) \equiv \sqrt{\frac{1}{h} \int_{-h}^0 \left(\frac{u(z)}{u(0)} - \frac{u_S(z)}{u_S(0)} \right)^2 dz}, \quad (19a)$$

$$F_w(\sigma, kh) \equiv \sqrt{\frac{1}{h} \int_{-h}^0 \left(\frac{w(z)}{w(0)} - \frac{w_S(z)}{w_S(0)} \right)^2 dz}, \quad (19b)$$

where the subscript S refers to the target velocities according to Stokes linear theory.

The velocity error F_u is shown as a function of σ for discrete values of kh in figure 1(a–c). Figure 1(a) shows the lower-order result with $N = 1$ (i.e. including second derivatives), figure 1(b) shows the higher order result with $N = 2$ and finally figure 1(c) shows the case of $N = 4$. Each of the figures clearly indicates a range of σ -values for which small errors occur even for relatively high kh -values: the optimal values are $\sigma = -0.562$ for $N = 1$, $\sigma = -0.672$ for $N = 2$ and $\sigma = -0.768$ for $N = 4$. For these specific choices, a 2% error in F_u is reached at a limiting kh of 1.81, 4.75

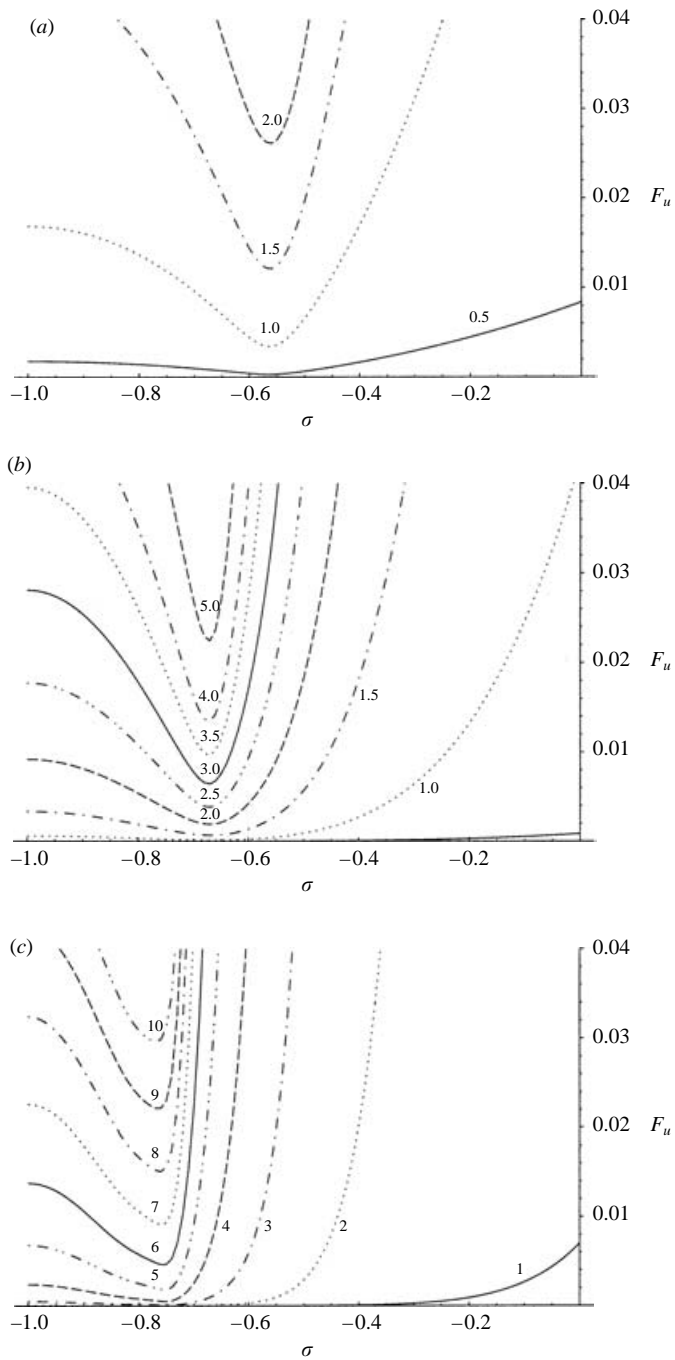


FIGURE 1. The error F_u as a function of σ for discrete values of kh . (a) First-order ($N=1$), (b) second-order ($N=2$) and (c) fourth-order ($N=4$) velocity profiles based on §3.1, i.e. (17a, b) and (18a–f).

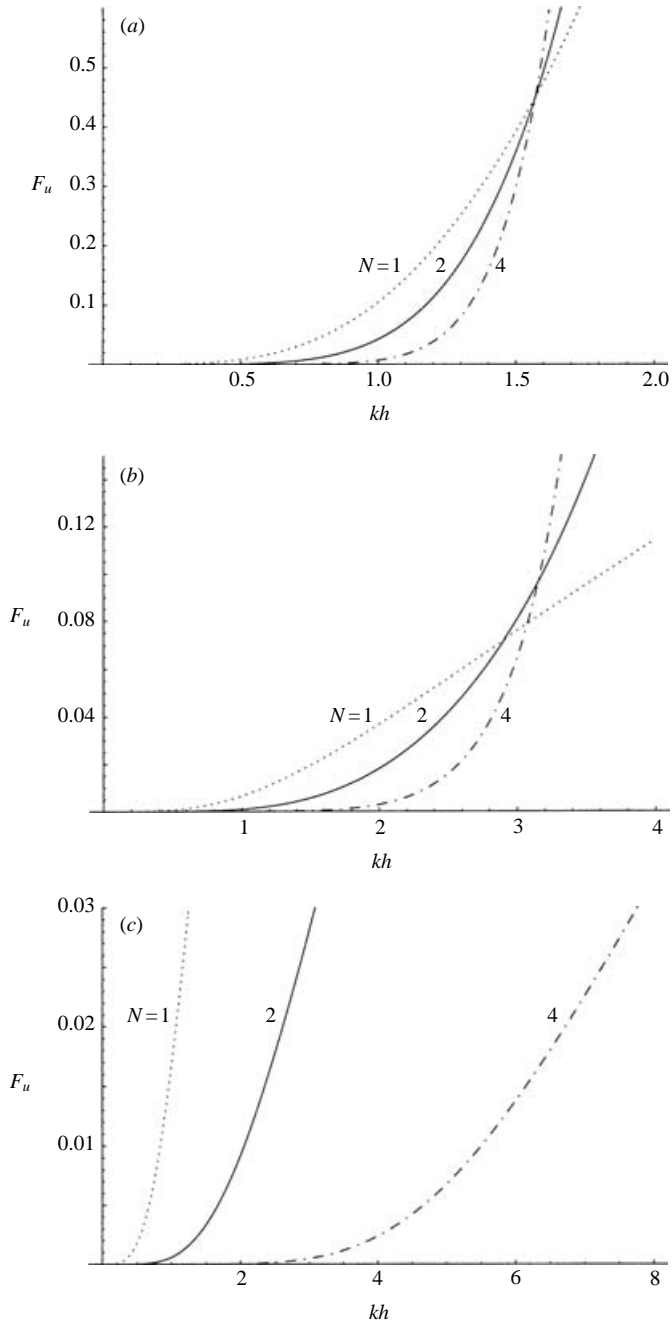


FIGURE 2. The error F_u as a function of kh for different orders of expansion. Velocity profile based on § 3.1, i.e. (17a, b) and (18a-f). (a) $\sigma = 1$, (b) $\sigma = -0.5$, (c) $\sigma = -1.0$.

and 8.71, respectively. The velocity error F_w has a similar variation and leads to the optimal choices of $\sigma = -0.635$ for $N = 1$, $\sigma = -0.717$ for $N = 2$ and $\sigma = -0.770$ for $N = 4$, for which the 2% error in F_w is reached at kh equal to 3.25, 5.39 and 10.66.

Figure 2(a-c) shows F_u as a function of kh for the classical choices of $\sigma = 0, -0.5$ and -1 . We notice from figure 2(a) that the case of $\sigma = 0$ leads to very poor accuracy

σ	$N=1$	$N=2$	$N=4$	Convergence radius
0	0.63, 0.94	0.88, 1.15	1.12, 1.30	$\pi/2$
-0.1	0.69, 1.02	0.97, 1.25	1.25, 1.42	$5\pi/9$
-0.2	0.76, 1.12	1.09, 1.38	1.42, 1.59	$5\pi/8$
-0.3	0.87, 1.26	1.26, 1.56	1.65, 1.81	$5\pi/7$
-0.4	1.06, 1.46	1.54, 1.81	2.00, 2.12	$5\pi/6$
-0.5	1.52, 1.83	2.06, 2.23	2.58, 2.61	π
-0.6	1.71, 2.92	3.16, 3.10	3.56, 3.52	$5\pi/4$
-0.7	1.32, 2.67	4.37, 5.27	5.87, 5.81	$5\pi/3$
-0.8	1.16, 2.16	3.14, 4.45	8.50, 10.04	$5\pi/2$
-0.9	1.09, 1.99	2.73, 3.80	7.25, 8.51	5π
-1.0	1.07, 1.95	2.62, 3.63	6.73, 7.84	∞

TABLE 1. Limiting wavenumbers kh_u, kh_w for which F_u, F_w exceed 2%. Based on velocity field in terms of \hat{u} , i.e. (17a, b) with (18a-f).

no matter how many terms we include and the three curves ($N = 1, 2$ and 4) intersect at $kh \approx 1.57$, beyond which the lower-order solution is better than the higher order. In figure 2(b) with the choice of $\sigma = -0.5$ (approximately the value used by Nwogu 1993) the applicability is clearly increased, but again the three curves ($N = 1, 2$ and 4) intersect, this time at $kh \approx 3.1$. The reason for the intersection of the curves in figure 2(a, b) is a lack of convergence, which will be discussed in further detail below. Finally, in figure 2(c) with $\sigma = -1$, we notice a continuous increase of accuracy for an increasing number of terms in the expansion. On the other hand, the accuracies achieved with $N=1$ and $N=2$ are quite poor. Table 1 summarizes the limiting kh values corresponding to 2% errors for a range of σ -values. The corresponding convergence criteria are also listed and they will be derived and discussed in the following.

3.1.2. Convergence of power series

Expressions derived from (8a, b) become power series approximations in Fourier space and hence they obey the classical convergence rules for Taylor series approximations. According to Hildebrand (1976, Chap. 10.7) (see also Baker & Graves-Morris 1981, Chap. 2.2, and Press *et al.* 1992 Chap. 5.1), we can state the following theorem:

THEOREM. *The Taylor series representation of a function has a radius of convergence which will equal the distance from the expansion point to the nearest point where the function encounters a singularity in the complex plane.*

Hence, any expansion of the velocity field in terms of \hat{u} will be governed by the singularities or simple poles of the target function (12a, b). These occur as complex roots of the denominator $\cosh(k(\hat{z} + h))$ and with $\hat{z} = \sigma h$ we find

$$kh_{Roots} = \frac{\pm i}{(1 + \sigma)} \left(\frac{\pi}{2} + n\pi \right), \quad n = 0, 1, 2, \dots \tag{20a}$$

As the power series representations of (12a, b) do not capture any of the poles in (20a), the convergence radius will be limited by

$$\hat{u} : kh_{Limit} = \frac{\pi}{2(1 + \sigma)}. \tag{20b}$$

We note that equation (20*b*) has previously been derived by Kennedy *et al.* (2002) on the basis of a direct analysis of the power series. When σ is decreased from 0 (still-water level), to -0.5 (mid-depth), to -0.75 , and finally to -1 (bottom), the convergence radius takes the values of $\pi/2$, π , 2π and eventually infinity. This is why the curves in figures 2(*a*) and 2(*b*) intersect, while we find no intersection in figure 2(*c*).

On the basis of (20*b*), we can now explain why the optimal choice of σ is pushed further and further towards -1 for an increasing number of terms in the expansion (figure 1*a-c*): from an extrapolation point of view, an expansion from the mid-depth (i.e. $\sigma = -0.5$) has the advantage that the maximum distance covered by the extrapolation (to the bottom and to the surface) becomes a minimum. As long as the order of the expansion is low this is what really matters. With increasing orders of the expansion, the accuracy is also increased but only within the convergence radius. Hence to utilize the full capacity of a certain high-order expansion, the convergence radius needs to be extended along with the order of the expansion. This calls for a gradual shift of the expansion point towards the sea bottom. The limit of $\sigma = -1$, where the convergence radius is unbounded, is reached when the order of the expansion goes to infinity.

3.2. Analysis of profiles expressed in terms of U

Many classical Boussinesq formulations have been expressed in terms of the depth-averaged horizontal velocity (see e.g. the reviews by Whitham 1974; Mei 1983; Madsen & Schäffer 1999). Generally, this variable involves the integral from the sea bottom to the instantaneous free surface, but in the present context where we consider only linear aspects of the velocity profiles, we only integrate up to the still-water datum. We can derive expressions for the velocity profile expanded in terms of U in the following way: insert (17*a, b*) in (13) and integrate to determine U in terms of \hat{u} ; invert this expression by using successive approximations, obtain an expression for \hat{u} in terms of U and insert the result in (17*a, b*) to obtain

$$u(x, y, z, t) = \sum_{n=0}^N \alpha_{2n} \nabla^{2n} U, \quad w(x, y, z, t) = \sum_{n=0}^N \beta_{2n+1} \nabla^{2n+1} U, \quad (21a, b)$$

with

$$\alpha_0 \equiv 1, \quad \alpha_2 \equiv -\frac{h^2}{3} - hz - \frac{z^2}{2}, \quad \alpha_4 \equiv -\frac{h^4}{45} + \frac{h^2 z^2}{6} + \frac{hz^3}{6} + \frac{z^4}{24}, \quad (22a, b, c)$$

$$\beta_1 \equiv -(z+h), \quad \beta_3 \equiv \frac{z^3}{6} + \frac{hz^2}{2} + \frac{h^2 z}{3}, \quad \beta_5 \equiv -\frac{z^5}{120} - \frac{hz^4}{24} - \frac{h^2 z^3}{18} + \frac{h^4 z}{45}. \quad (22d, e, f)$$

Again the order of derivatives kept in w is one higher than the order kept in u , in contrast to traditional Boussinesq formulations, where it is the opposite.

We note that lower-order expressions (with $N=1$) were given by e.g. Boussinesq (1872), Serre (1953), Peregrine (1967), Su & Gardner (1969), Benjamin *et al.* (1972), Whitham (1973), Mei (1983), and Dingemans (1997). Of these, only Dingemans (in eq. 5.462*f*, Chapter 5.11.3) included a β_3 contribution, but it differs from (22) due to typographical errors. Higher-order expressions with $N=2$ appear in Dingemans (1997) and in Madsen & Schäffer (1998, 1999) but without the β_5 terms.

In Fourier space, (21*a, b*) and (22*a-f*) agree with a Taylor series expansion in kh of the target solution (14*a, b*), and high-order expansions valid on a constant depth

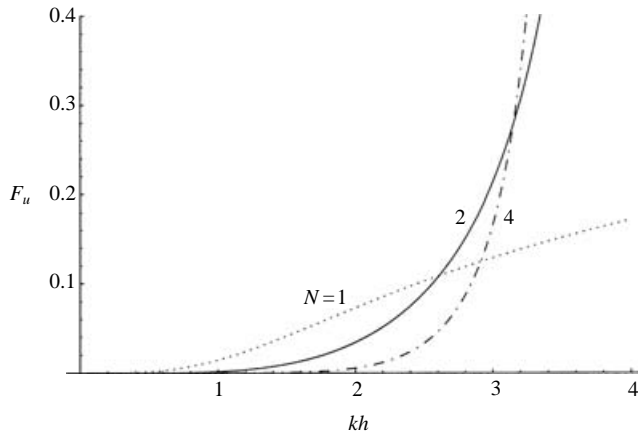


FIGURE 3. The error F_u as a function of kh for different orders of expansion. Velocity profile based on § 3.2, i.e. (21a, b) and (22a–f).

$N = 1$	$N = 2$	$N = 4$	Convergence radius
1.13, 1.52	1.77, 1.98	2.36, 2.41	π

TABLE 2. Limiting wave numbers kh_u, kh_w for which F_u, F_w exceed 2%. Based on velocity field in terms of U , i.e. (21a, b) with (22a–f).

can easily be derived by using (14a, b) as a starting point. The velocity errors are quantified by using (19a, b). Figure 3 shows the errors of F_u as a function of kh for the three orders of expansion ($N = 1, 2$ and 4). We notice that the higher-order curves intersect at $kh \approx 3.1$ indicating a lack of convergence. According to the theorem from § 3.1, convergence will not occur beyond the simple poles of the target function (14a, b). These appear as the complex roots of the denominator $\sinh(kh)$ which are

$$kh_{Roots} = \pm in\pi, \quad n = 0, 1, 2, \dots, \tag{23a}$$

i.e. the convergence radius for the method becomes

$$U : \quad kh_{Limit} = \pi. \tag{23b}$$

Table 2 summarizes the limiting kh -values corresponding to 2% errors in u and w , respectively. Note that the accuracy is slightly worse than achieved with $\sigma = -0.5$ in table 1.

3.3. Analysis of profiles expressed in terms of a pseudo-velocity variable

As our last example of Boussinesq expansions expressed in terms of a horizontal velocity variable, we discuss and analyse the approach by Gobbi *et al.* (2000). They used a new dependent variable \tilde{u} which was defined as the weighted average of the horizontal velocity at two distinct z -levels i.e.

$$\tilde{u} \equiv \beta u(z_a) + (1 - \beta)u(z_b). \tag{24}$$

They expanded the velocity field in terms of this variable and obtained

$$\mathbf{u}(x, y, z, t) = \sum_{n=0}^N \alpha_{2n} \nabla^{2n} \tilde{\mathbf{u}}, \quad w(x, y, z, t) = \sum_{n=0}^N \beta_{2n+1} \nabla^{2n+1} \tilde{\mathbf{u}}, \quad (25a, b)$$

where

$$\alpha_0 \equiv 1, \quad \alpha_2 \equiv \frac{h^2}{2} \left(B - \left(1 + \frac{z}{h} \right)^2 \right), \quad (26a, b)$$

$$\alpha_4 \equiv \frac{h^4}{4} \left(B^2 - \frac{D}{6} - B \left(1 + \frac{z}{h} \right)^2 + \frac{1}{6} \left(1 + \frac{z}{h} \right)^4 \right), \quad (26c)$$

$$\beta_1 \equiv -(z + h), \quad \beta_3 \equiv \frac{h^3}{2} \left(-B \left(1 + \frac{z}{h} \right) + \frac{1}{3} \left(1 + \frac{z}{h} \right)^3 \right), \quad (26d, e)$$

$$\beta_5 \equiv -\frac{h^5}{4} \left(\left(B^2 - \frac{D}{6} \right) \left(1 + \frac{z}{h} \right) - \frac{B}{3} \left(1 + \frac{z}{h} \right)^3 + \frac{1}{30} \left(1 + \frac{z}{h} \right)^5 \right), \quad (26f)$$

and

$$B \equiv \beta \left(1 + \frac{z_a}{h} \right)^2 + (1 - \beta) \left(1 + \frac{z_b}{h} \right)^2, \quad D \equiv \beta \left(1 + \frac{z_a}{h} \right)^4 + (1 - \beta) \left(1 + \frac{z_b}{h} \right)^4. \quad (27a, b)$$

Again the order of derivatives kept in w is one higher than the order kept in u , in contrast to traditional Boussinesq formulations, where it is the opposite. This means that we have included a β_5 term, although this was omitted by Gobbi *et al.* (2000).

For $\beta = 1$, (26a–f) simplify to the coefficients given in (18a–f), and for $N = 1$ we recover Nwogu’s (1993) lower-order formulation. Gobbi *et al.* (2000) introduced two arbitrary levels to improve the linear dispersion relation and found that a Padé (4,4) approximation to the target solution could be achieved (see figure 12) with the choice of $B = 1/9$ and $D = 5/189$. For this choice they solved for parameters β, z_a, z_b . With three unknowns and only two constraints this gave them an infinite number of solutions, leading to

$$\frac{z_a}{h} \equiv \left(\frac{1}{9} - \sqrt{\frac{8\beta}{567(1-\beta)}} + \sqrt{\frac{8}{567\beta(1-\beta)}} \right)^{1/2} - 1, \quad (28a)$$

$$\frac{z_b}{h} \equiv \left(\frac{1}{9} - \sqrt{\frac{8\beta}{567(1-\beta)}} \right)^{1/2} - 1. \quad (28b)$$

Only for β between 0.018 and 0.467, did both levels z_a and z_b fall inside the water column, and Gobbi & Kirby (1999) recommended the value $\beta = 0.2$ for which (28a, b) yields $z_a = -0.41h$ and $z_b = -0.77h$. This corresponds to a weighted-average level of $\hat{z} \approx -0.7h$.

In Fourier space, (25a, b) and (26a–f) agree with a Taylor series expansion in kh of the target solution

$$\frac{u_s(z)}{\tilde{u}_s} \equiv \frac{\cosh(k(z + h))}{\beta \cosh(k(z_a + h)) + (1 - \beta) \cosh(k(z_b + h))}. \quad (29)$$

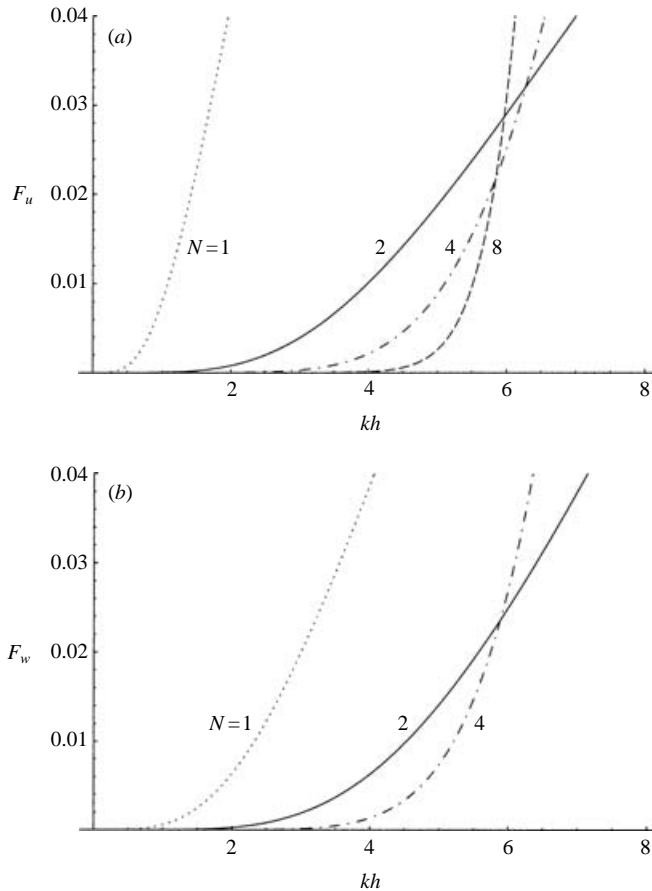


FIGURE 4. (a) The error F_u and (b) F_w as a function of kh for different orders of expansion. Velocity profile based on §3.3, i.e. (25a, b) and (26a–f).

While Gobbi *et al.* (2000) considered the case of $N=2$, we use (29) as a starting point for Taylor expansions to the order of $N=1, 2, 4$ and 8 . In this process we keep the choice of B and D fixed at $1/9$ and $5/189$, respectively. From a linear dispersion point of view, this may not be the optimal choice for N different from 2 , but as our objective here is merely to investigate the capacity of higher and lower order expansions for internal kinematics, we have chosen to do so. The velocity errors are quantified by using (19a, b).

Figure 4(a, b) shows the errors of F_u and F_w as functions of kh for the four orders of expansions ($N=1, 2, 4$ and 8). Note that the formulation by Gobbi *et al.* (2000) corresponds to $N=2$ in figure 4(a) and $N=1$ in figure 4(b) because they neglected the β_5 term in (26f). This clearly makes their w -profile less accurate than their u -profile, a fact which could also be observed in their figures 5 and 6. On the other hand, the profiles obtained with $N=2$ in u as well as in w are indeed very accurate. From figure 4(a, b) we notice that the three high-order curves intersect at $kh \approx 5.88$ indicating a lack of convergence.

Recently, Kennedy *et al.* (2002) discussed convergence in connection with the velocity profile of Gobbi *et al.*, but they did not give any explicit measures for it.

$N = 1$	$N = 2$	$N = 4$	Convergence radius
1.42, 3.00	5.13, 5.58	5.76, 5.75	5.85

TABLE 3. Limiting wavenumbers kh_u, kh_w for which F_u, F_w exceed 2%. Based on velocity field in terms of \tilde{u} , i.e. (25a, b) with (26a-f).

Here we simply apply the theorem from §3.1, according to which convergence will not occur beyond the simple poles of the target function (29). These appear as the complex roots of the denominator of (29) which leads to

$$\tilde{u}: kh_{Limit} = 5.85, \tag{30}$$

i.e. in good agreement with the observed point of intersection.

Table 3 summarizes the limiting kh values corresponding to 2% errors in u and w . For $N = 1$ there is little difference between table 3 and the best choices from the corresponding column in table 1. However, for $N = 2$ (which is the case considered by Gobbi *et al.*) the results in table 3 are clearly better than the results from the same column in table 1. Finally, for $N = 4$, the best choices from table 1 are superior to table 3. The reason for this is this following: by comparing (30) and (20b), we notice that only for $-0.73 \leq \sigma \leq -1$ is the convergence radius larger in method (17a, b) than in method (25a, b), and this implies that only very high-order expansions will be more accurate with (17a, b) than with (25a, b).

4. Truncated series solutions in terms of \hat{u} and \hat{w}

The formulations discussed so far have all been limited by a finite radius of convergence, except for the case of (17a, b) with $\hat{z} = -h$. It turns out that the radius of convergence can be significantly increased if we avoid a power series approximation to the tan-operator in (7) and (8a, b). Hence, instead of the explicit determination and elimination of \hat{w} , which is done in almost all previous Boussinesq formulations, we keep \hat{w} as one of the expansion parameters and solve (4a, b) and (6) along with the rest of the model equations. Such a concept was first proposed by Agnon *et al.* (1999) using $\hat{z} = 0$, and later by Madsen *et al.* (2002a, b) using $\hat{z} = \sigma h$.

4.1. Using Taylor series approximations for cos- and sin-operators

In this section, we consider Method I from Madsen *et al.* (2002b) and introduce power series approximations to the cos- and sin-operators in (6) and (4a, b). By following this approach instead of the one discussed in §3.1, we can represent the tan-operator in (7) by a rational function of a power series for the sin-operator divided by the power series for the cos-operator. In Fourier space, this leads to the combination of (10a, b) and (11) and after the elimination of C_1 we obtain

$$\frac{u(x, z, t)}{\hat{u}} = \cosh(k(z - \hat{z})) + \sinh(k(z - \hat{z})) \frac{\sinh(k(h + \hat{z}))}{\cosh(k(h + \hat{z}))}, \tag{31a}$$

$$\frac{w(x, z, t)}{i\hat{u}} = \sinh(k(z - \hat{z})) + \cosh(k(z - \hat{z})) \frac{\sinh(k(h + \hat{z}))}{\cosh(k(h + \hat{z}))}. \tag{31b}$$

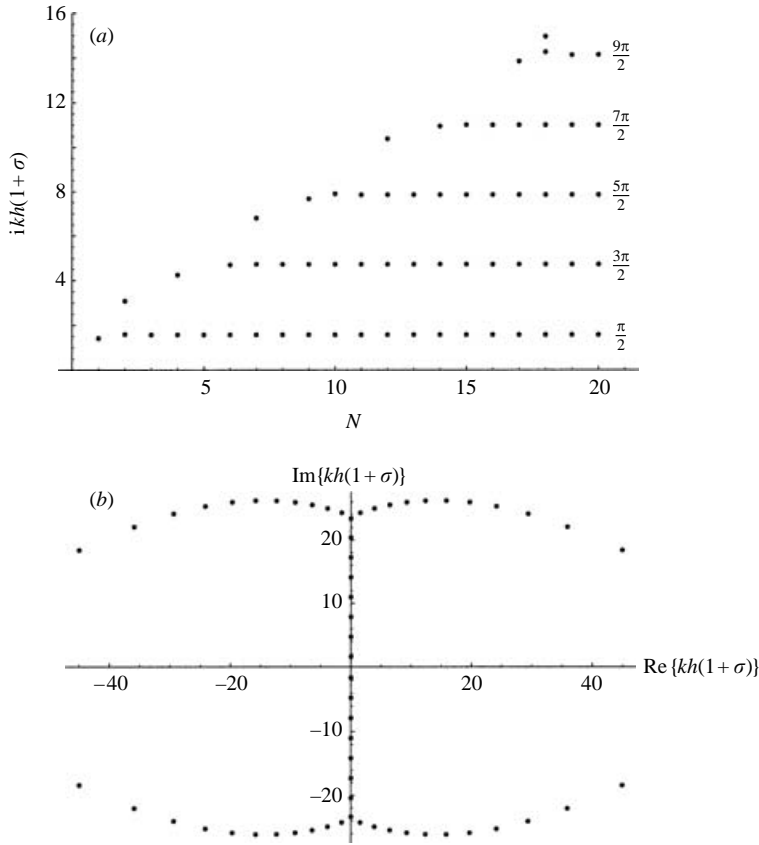


FIGURE 5. (a) Pure imaginary roots of Taylor series expansions from $kh=0$ of $\cosh(kh(1+\sigma))$. Horizontal axis: N , the order of the expansion including $O(k^{2N})$ terms. (b) Corresponding complex roots. Order of expansion, $N=30$ i.e. including $O(k^{60})$ terms.

Applying truncated sin- and cos-operators corresponds to using truncated series expansions of sinh and cosh in (31a, b). When infinite series expansions are applied, (31a, b) are identical to the target functions (12a, b).

4.1.1. Convergence of series solutions

As discussed in § 3.1, the convergence of a power series is governed by the distance to the nearest complex pole of the target function. If, however, the power series is combined with or replaced by fractions of power series, which capture the nearest singularities, the convergence radius of the approximation is extended to the next singularity. In (31a, b) this happens due to the fraction containing the cosh-denominator. With increasing orders of the approximation, (31a, b) will gradually capture more and more poles, and in the asymptotic limit the convergence radius becomes infinity.

Figure 5(a) shows the poles which can be captured as a function of N , the order of the expansion: for $N=1$ a pole at $ikh(1+\sigma)=\pm i 1.4142$ is found, approximating the correct pole at $\pm i \pi/2$. For $N=2$ the first pole is corrected to $\pm i 1.5925$ and a second pole is found at $\pm i 3.0764$ (giving a poor estimate of the correct pole at $\pm i 3\pi/2$). For $N=4$ the first pole is further corrected to $\pm i 1.5708$, while the second

pole is corrected to $\pm i 4.2408$. As seen from figure 5(a), a third pole appears for $N = 7$, a fourth pole for $N = 12$ and a fifth pole for $N = 17$.

In addition to the pure imaginary roots, the Taylor series expansions contain a number of false roots which are distributed in the complex plane. This is illustrated in figure 5(b), which shows all the complex roots for the case of $N = 30$.

4.1.2. Accuracy of velocity profiles

The velocity error F_u is shown as a function of σ for discrete values of kh in figures 6(a) ($N = 1$), 6(b) ($N = 2$) and 6(c) ($N = 4$). Each of the figures clearly indicate a range of σ -values for which small errors occur even for relatively high kh -values. Note that in contrast to figure 1(a-c), the optimal choice of σ is no longer sensitive to the order of the expansion and a position close to mid-depth is always preferable from an accuracy point of view: based on F_u the optimal σ -values are found to be $\sigma = -0.519$ for $N = 1$, $\sigma = -0.533$ for $N = 2$ and $\sigma = -0.526$ for $N = 4$ and for these choices of σ , a 2% error in F_u is reached at a limiting kh of 2.85 ($N = 1$), 6.14 ($N = 2$) and 14.87 ($N = 4$). Based on F_w the optimal values become $\sigma = -0.488$ for $N = 1$, $\sigma = -0.484$ for $N = 2$ and $\sigma = -0.484$ for $N = 4$ and for these choices of σ , a 2% error in F_w is reached at a limiting kh of 2.82 ($N = 1$), 6.84 ($N = 2$) and 16.57 ($N = 4$). For the case of $\sigma = 0$, the 2% error limits in (F_u, F_w) are reached at $kh = (0.98, 1.25)$ for $N = 1$, at $kh = (1.73, 2.04)$ for $N = 2$, and at $kh = (3.33, 3.70)$ for $N = 4$.

In comparison with § 3.1, we note that for the case of $N = 1$ the improvement is moderate, but for $N = 2$ and $N = 4$ the kh -values have increased significantly. Table 4 summarizes the kh values corresponding to 2% errors in u and w for a range of σ -values. In comparison with table 1, the accuracy is improved for most combinations of σ and N , except for the interval of $-0.8 \leq \sigma \leq -1$, where the improvement is either small or absent.

Figure 7 shows the error of F_u as a function of kh for the case of $\sigma = -0.5$ using the three orders of expansions ($N = 1, 2$ and 4). We notice a continuous increase of accuracy for an increasing number of terms in the expansion, and the curves do not intersect due to the unlimited convergence radius.

4.2. Introducing Padé approximants in the kinematic bottom condition

It is well-known that Padé approximants generally have superior accuracy compared to power series approximations and such techniques have successfully been used in the framework of Boussinesq theory to enhance the accuracy of the linear dispersion relation, see e.g. Witting (1984), Madsen *et al.* (1992), Nwogu (1993) and Madsen & Schäffer (1998). In the pursuit of differential equations with imbedded Padé-type dispersion properties, a number of different procedures have been applied. Of these, the method by Agnon *et al.* (1999) is the most general and direct. They start from (4a, b) with $\hat{z} = 0$, and show that the accuracy of the kinematic bottom condition (6) determines the accuracy of linear dispersion. To enhance this accuracy they introduce a linear operator of the form

$$L(\lambda \nabla) \equiv 1 + \sum_{n=1}^{2N} \delta_{2n} \lambda^{2n} \nabla^{2n}, \quad (32)$$

and apply it to equation (6), which consequently is modified to

$$\cos(\lambda \nabla) L(\lambda \nabla) \hat{w} + \sin(\lambda \nabla) L(\lambda \nabla) \hat{u} = 0, \quad (33)$$

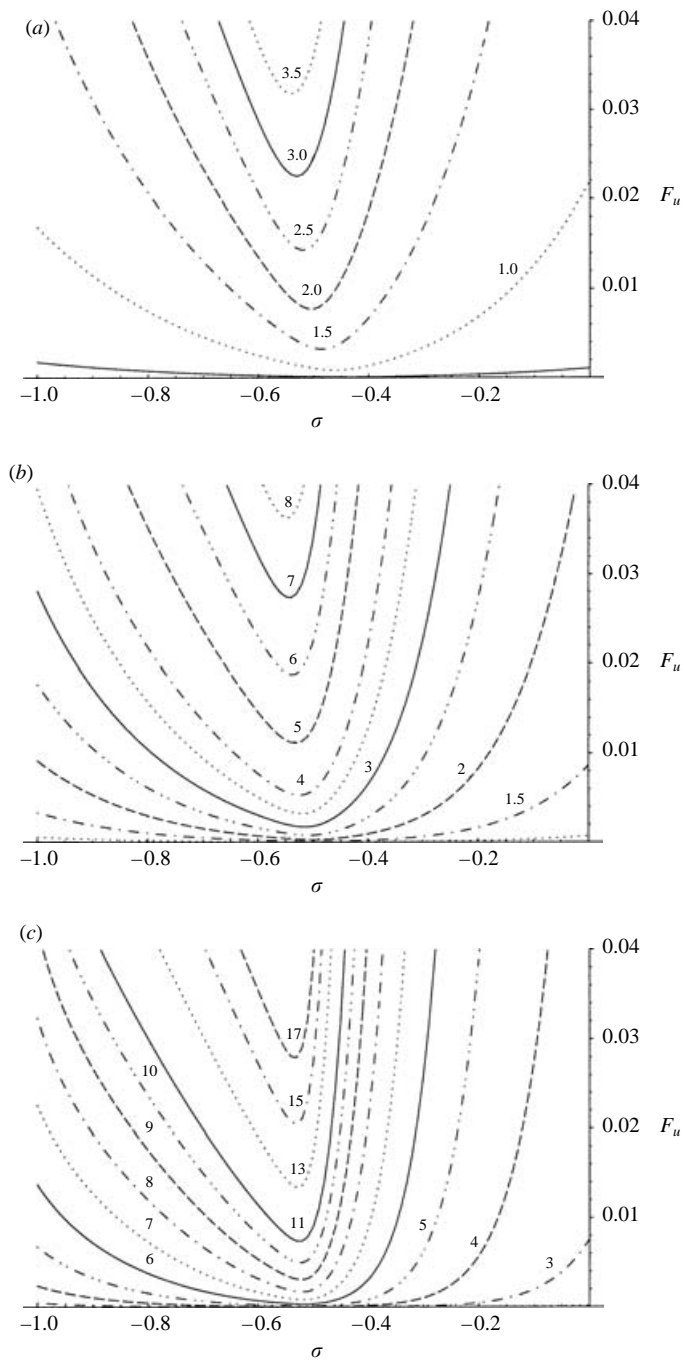


FIGURE 6. The error F_u shown as a function of σ for discrete values of kh . (a) First-order ($N = 1$), (b) second-order ($N = 2$) and (c) fourth-order ($N = 4$) velocity profiles based on § 4.1, i.e. (4a, b) and (6), or (31a, b) in Fourier space.

σ	$N = 1$	$N = 2$	$N = 4$	Convergence radius
0	0.98, 1.25	1.73, 2.04	3.33, 3.70	∞
-0.1	1.12, 1.44	1.99, 2.38	3.87, 4.34	∞
-0.2	1.30, 1.69	2.36, 2.89	4.63, 5.29	∞
-0.3	1.57, 2.07	2.93, 3.72	5.80, 6.86	∞
-0.4	2.05, 2.58	3.91, 5.45	7.95, 10.44	∞
-0.5	2.79, 2.81	5.78, 6.75	13.60, 16.19	∞
-0.6	2.46, 2.58	5.65, 5.64	13.24, 13.21	∞
-0.7	1.84, 2.30	4.65, 4.74	11.02, 11.02	∞
-0.8	1.48, 2.10	3.86, 4.14	9.41, 9.44	∞
-0.9	1.24, 1.99	3.19, 3.77	8.08, 8.33	∞
-1.0	1.07, 1.95	2.62, 3.63	6.73, 7.84	∞

TABLE 4. Limiting wavenumbers kh_u, kh_w for which F_u, F_w exceed 2%. Based on velocity field in terms of \hat{u} and \hat{w} , i.e. (4a, b) with (6), or (31a, b).

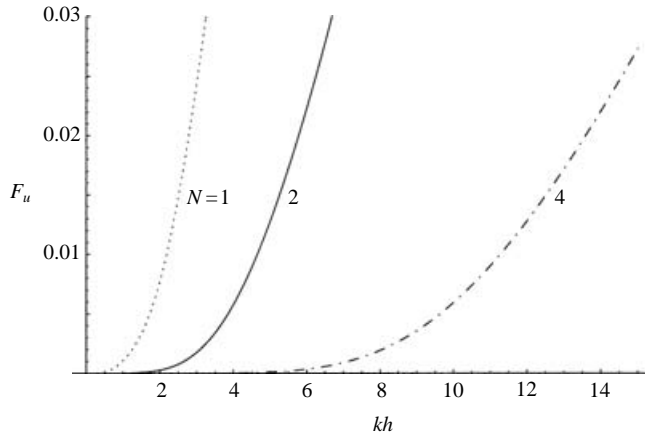


FIGURE 7. The error F_u for $\sigma = -0.5$, shown as a function of kh for different orders of expansion. Velocity profile based on §4.1, i.e. (4a, b) and (6), or (31a, b) in Fourier space.

with $\lambda = h$. The δ_{2n} coefficients in (32) are determined by truncating the infinite cos- and sin-operators at $4N$ and $4N + 1$, multiplying each of the series by (32), and requiring that all terms with powers of $2N + 2$ to $4N + 1$ vanish. For the case of $N = 1$, this procedure yields

$$\delta_2 = \frac{1}{10}, \quad \delta_4 = \frac{1}{120}, \tag{34a, b}$$

$$\cos(\lambda \nabla) L(\lambda \nabla) = 1 - \frac{2\lambda^2 \nabla^2}{5} + O(\lambda^6 \nabla^6), \tag{34c}$$

$$\sin(\lambda \nabla) L(\lambda \nabla) = \lambda \nabla - \frac{\lambda^3 \nabla^3}{15} + O(\lambda^7 \nabla^7), \tag{34d}$$

while $N = 2$ leads to

$$\delta_2 = \frac{1}{18}, \quad \delta_4 = \frac{1}{504}, \quad \delta_6 = \frac{1}{15120}, \quad \delta_8 = \frac{1}{362880}, \tag{35a-d}$$

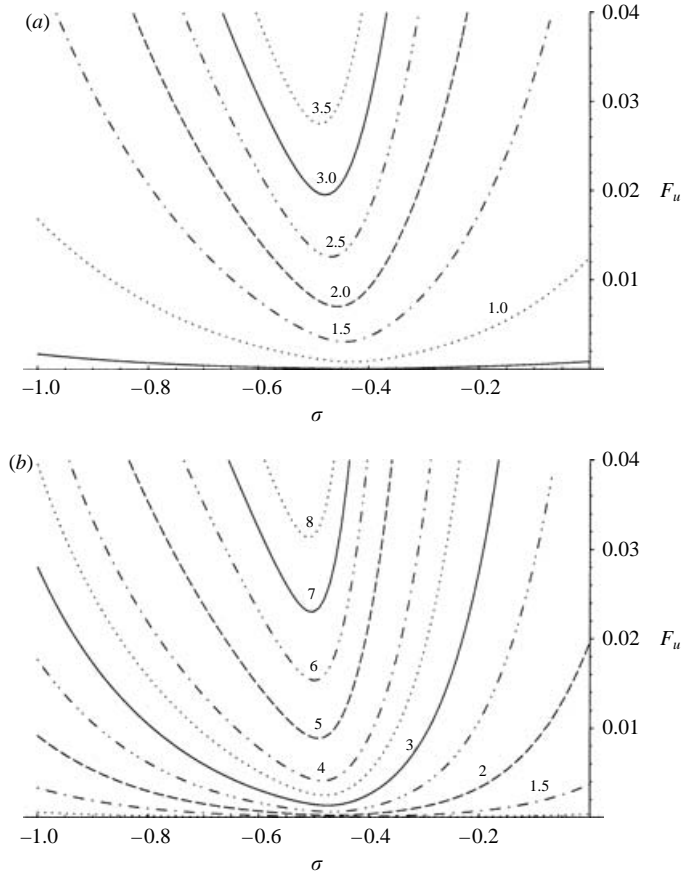


FIGURE 8. The error F_u as a function of σ for discrete values of kh . (a) First-order ($N = 1$) and (b) second-order ($N = 2$) velocity profiles based on §4.2.

$$\cos(\lambda\nabla)L(\lambda\nabla) = 1 - \frac{4\lambda^2\nabla^2}{9} + \frac{\lambda^4\nabla^4}{63} + O(\lambda^{10}\nabla^{10}), \quad (35e)$$

$$\sin(\lambda\nabla)L(\lambda\nabla) = \lambda\nabla - \frac{\lambda^3\nabla^3}{9} + \frac{\lambda^5\nabla^5}{945} + O(\lambda^{11}\nabla^{11}). \quad (35f)$$

We note that in (34c,d) as well as in (35e,f) the accuracy has become twice the order of the terms included, which is a typical property of Padé approximants. With this procedure, Agnon *et al.* (1999) enhanced the accuracy of the kinematic bottom condition and achieved Padé (2,2) or Padé (4,4) dispersion characteristics for $N = 1$ and $N = 2$, respectively. However, as they used $\hat{z} = 0$, the underlying velocity profile was actually quite inaccurate.

Recently, Madsen *et al.* (2002b), in their Method 2, generalized the approach to the case of arbitrary \hat{z} , i.e. they use (4a,b) combined with (33) with $\lambda = h + \hat{z}$. In Fourier space, the resulting velocity profile becomes similar to (31a,b) with the exception that Taylor approximations are used only in the cosh/sinh functions with arguments $z - \hat{z}$, while the approximations (34c,d) or (35e,f) are used in functions with arguments $h + \hat{z}$.

The resulting velocity error F_u is shown as a function of σ for discrete values of kh in figure 8(a) ($N = 1$) and figure 8(b) ($N = 2$). For F_u as well as for F_w

the optimal σ -values become $\sigma = -0.469$ ($N = 1$) and $\sigma = -0.494$ ($N = 2$) for which the 2% errors are reached at kh equal to (3.03, 3.12) and (6.61, 6.62), respectively. Note that these kh -values are only marginally larger than the ones obtained in §4.1, and by comparing figure 8(a, b) with figure 6(a, b), we conclude that the increased accuracy of the kinematic bottom condition has had little effect on the accuracy of the velocity profile. However, as shown in figure 12 and discussed in §6, the improved accuracy of the kinematic bottom condition has a major effect on the linear dispersion relation.

4.3. *Further introduction of Padé approximants by the use of pseudo-velocities*

With the objective of introducing Padé approximants in the velocity profile, Madsen *et al.* (2002a, b) introduced their Method 3, which will be summarized in the following. The starting point is again (4a, b), but now the physical velocities \hat{u} , \hat{w} are expanded in terms of the pseudo-velocities \hat{u}^* , \hat{w}^* , which are defined by the relations $\hat{u} \equiv L(\hat{z}\nabla)\hat{u}^*$ and $\hat{w} \equiv L(\hat{z}\nabla)\hat{w}^*$, with the L-operator given by (32) and (34a, b) or (35a–d). Inserting these definitions in (4a, b) yields

$$u(x, y, z, t) = \cos((z - \hat{z})\nabla)L(\hat{z}\nabla)\hat{u}^* + \sin((z - \hat{z})\nabla)L(\hat{z}\nabla)\hat{w}^*, \tag{36a}$$

$$w(x, y, z, t) = \cos((z - \hat{z})\nabla)L(\hat{z}\nabla)\hat{w}^* - \sin((z - \hat{z})\nabla)L(\hat{z}\nabla)\hat{u}^*. \tag{36b}$$

Note that at $z = 0$, where the arguments of the L-, cos- and sin-operators coincide, the formal accuracy of (36a, b) will be doubled, in agreement with (34c, d) for $N = 1$ and with (35e, f) for $N = 2$. For other values of the z -coordinate, the formal accuracy of (36a, b) is no higher than without the enhancement. However, the effective accuracy of (36a, b) turns out to be superior to (4a, b) as demonstrated in the following.

We insert (32) in (36a, b), with (34a, b) for $N = 1$, and with (35a–d) for $N = 2$, and obtain

$$u(x, y, z, t) = \sum_{n=0}^N \alpha_{2n} \nabla^{2n} \hat{u}^* + \sum_{n=0}^N \beta_{2n+1} \nabla^{2n+1} \hat{w}^*, \tag{37a}$$

$$w(x, y, z, t) = \sum_{n=0}^N \alpha_{2n} \nabla^{2n} \hat{w}^* - \sum_{n=0}^N \beta_{2n+1} \nabla^{2n+1} \hat{u}^*, \tag{37b}$$

where the first two coefficients are identical to the Taylor coefficients from (5), i.e. $\alpha_0 \equiv 1$, $\beta_1 \equiv (z - \hat{z})$, while the other coefficients will depend on the order of the truncation. The case of $N = 1$ leads to

$$\alpha_2 \equiv -\frac{(z - \hat{z})^2}{2} + \frac{\hat{z}^2}{10}, \quad \beta_3 \equiv -\frac{(z - \hat{z})^3}{6} + \frac{\hat{z}^2(z - \hat{z})}{10}, \tag{38a, b}$$

while $N = 2$ leads to

$$\alpha_2 \equiv -\frac{(z - \hat{z})^2}{2} + \frac{\hat{z}^2}{18}, \quad \alpha_4 \equiv \frac{(z - \hat{z})^4}{24} - \frac{\hat{z}^2(z - \hat{z})^2}{36} + \frac{\hat{z}^4}{504}, \tag{39a, b}$$

$$\beta_3 \equiv -\frac{(z - \hat{z})^3}{6} + \frac{\hat{z}^2(z - \hat{z})}{18}, \quad \beta_5 \equiv \frac{(z - \hat{z})^5}{120} - \frac{\hat{z}^2(z - \hat{z})^3}{108} + \frac{\hat{z}^4(z - \hat{z})}{504}. \tag{39c, d}$$

At the sea bottom, Madsen *et al.* (2002a, b) manipulated the kinematic condition with another linear operator to obtain the attractive relations given in (34c, d) for

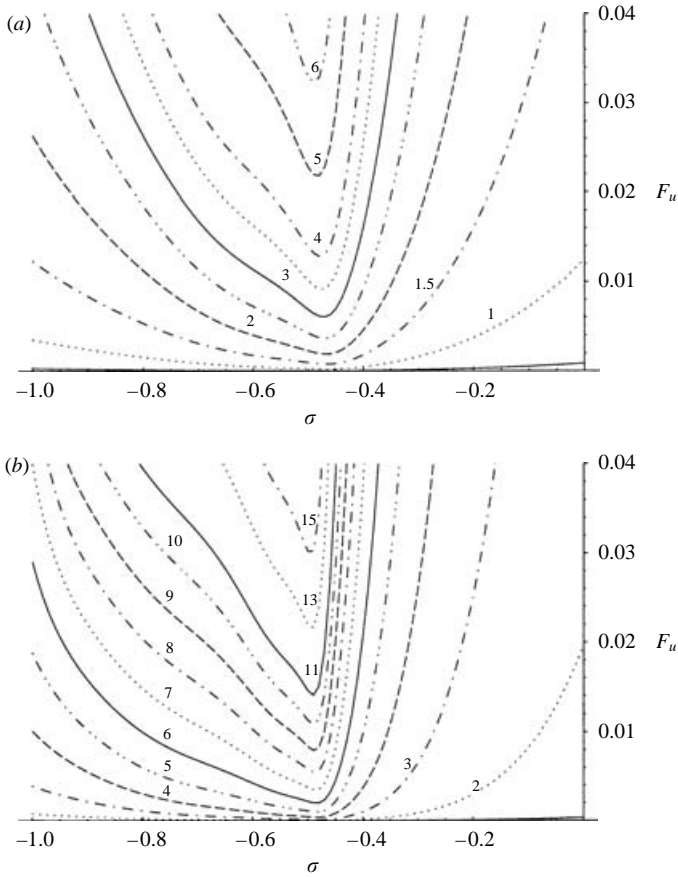


FIGURE 9. The error F_u as a function of σ for discrete values of kh . (a) First-order ($N=1$) and (b) second-order ($N=2$) velocity profiles based on §4.3, i.e. (37a,b) and (38a,b) for (a) and (37a,b) and (39a–d) for (b).

$N=1$ and in (35e, f) for $N=2$. For the case of $N=2$ this resulted in

$$\left(1 - \frac{4\lambda^2 \nabla^2}{9} + \frac{\lambda^4 \nabla^4}{63}\right) \hat{w}^* + \left(\lambda \nabla - \frac{\lambda^3 \nabla^3}{9} + \frac{\lambda^5 \nabla^5}{945}\right) \hat{u}^* = 0, \quad (40)$$

where $\lambda \equiv h + \hat{z}$.

4.3.1. Accuracy of velocity profiles

To compare the profiles of (37a,b) with Stokes target solution, we first solve (40) in Fourier space to express \hat{w}^* as a rational function involving \hat{u}^* . Next, we eliminate \hat{w}^* from (37a,b) and express the velocity profiles in terms of \hat{u}^* . Finally, we determine the ratios $u(z)/u(0)$ and $w(z)/w(0)$ and insert in (19a,b). The velocity error F_u is shown as a function of σ for discrete values of kh in figures 9(a) ($N=1$) and 9(b) ($N=2$). As mentioned above, the enhancement technique has doubled the formal accuracy of the kinematic bottom condition and of the profile at $z=0$, and as a result we notice a significant improvement in the velocity errors: figure 9(a) (with $N=1$) resembles figure 6(b) (with $N=2$), and figure 9(b) (with $N=2$) resembles figure 6(c) (with $N=4$).

σ	$N = 1$ (37a, b), (38a, b)	$N = 2$ (37a, b), (39a-d)	$N = 2$ § 5 (A)
0	1.13, 1.18	2.01, 2.02	4.38, 5.00
-0.1	1.32, 1.40	2.35, 2.37	5.24, 6.10
-0.2	1.60, 1.71	2.88, 2.90	6.52, 7.85
-0.3	2.10, 2.27	3.79, 3.81	8.63, 11.03
-0.4	3.23, 3.65	5.96, 6.04	12.55, 17.18
-0.5	4.71, 4.48	12.49, 12.22	16.03, 20.99
-0.6	3.84, 3.90	10.36, 10.36	10.94, 17.18
-0.7	3.27, 3.51	8.89, 8.89	7.86, 11.03
-0.8	2.60, 3.11	7.95, 7.97	6.17, 7.85
-0.9	2.12, 2.71	6.70, 6.98	5.11, 6.10
-1.0	1.80, 2.24	5.13, 5.58	4.39, 5.00

TABLE 5. Limiting wavenumbers kh_u, kh_w for which F_u, F_w exceed 2%. Based on the velocity field from § 4.3 (last column from § 5, transformation A).

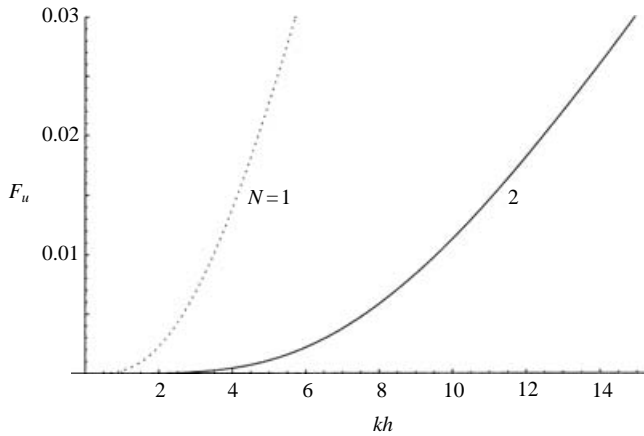


FIGURE 10. The error F_u for $\sigma = -0.5$, as a function of kh for different orders of expansion. Velocity profile based on § 4.3, i.e. (37a, b) with (38a, b) and (39a-d).

Table 5 summarizes the kh -values corresponding to 2% errors in u and w for a range of σ -values (the last column lists results from the method derived in § 5). In the interval $0 \geq \sigma \geq -0.4$ the improvement over table 4 is actually quite moderate, but for $-0.4 > \sigma \geq -1$ and especially near $\sigma \approx -0.5$ we notice a significant improvement for $N = 1$ and $N = 2$. For the case of $\sigma = 0$, the 2% error limits in (F_u, F_w) are reached at $kh = (1.13, 1.18)$ for $N = 1$, and at $kh = (2.01, 2.02)$ for $N = 2$. For F_u as well as for F_w the optimal σ -values become $\sigma = -0.480$ ($N = 1$) and $\sigma = -0.489$ ($N = 2$) for which the 2% errors are reached at kh equal to (4.82, 4.64) and (12.59, 12.48), respectively. This is 52% increase for $N = 1$ and 95% increase for $N = 2$ in comparison with the results obtained without the enhancement (see § 4.1).

Figure 10 shows the error of F_u as function of kh for the case of $\sigma = -0.5$. It is clear that the curve for $N = 1$ lies between curves $N = 2$ and $N = 1$ in figure 7, while the curve for $N = 2$ is only slightly less accurate than $N = 4$ in figure 7. The curves for F_w are very similar and are not shown. Finally, it should be mentioned that the

imbedded linear dispersion relation has superior accuracy as shown in figure 12, and discussed in §6.

5. A new formulation doubling the relative order of the vertical coordinate

Throughout §§3 and 4, formulations have been given on the form $z^n \nabla^n$, i.e. the polynomial order of the vertical coordinate has been the same as the order of the horizontal gradient operator. It turns out, however, to be possible to double the polynomial order of z without increasing the order of the horizontal derivatives. In the following, we derive a new formulation which is an extension to the method from §4.3.

In §4.3, we introduced the pseudo-velocity variables \hat{u}^* and \hat{w}^* , defined by the relations $\hat{u} \equiv L(\hat{z}\nabla)\hat{u}^*$ and $\hat{w} \equiv L(\hat{z}\nabla)\hat{w}^*$, with the L-operator given by (32). As a result the velocity field, for the case of $N=2$, was given by (37a, b) and (39a–d), which involved up to fifth-order powers in ∇ as well as fifth-order powers in z and \hat{z} . The objective in the following is to modify these expressions by including up to tenth-order powers of z and \hat{z} without increasing the order of the horizontal derivatives in (37a, b).

As a starting point, we introduce the pseudo-velocity potential Φ^* defined by the relation

$$\Phi(x, y, z, t) = L(\hat{z}\nabla) \Phi^*(x, y, z, t). \quad (41)$$

On a constant depth, which is considered throughout this paper, \hat{z} will be constant and the L-operator will commute with the gradient operator. This leads to

$$u \equiv \nabla\Phi = L(\hat{z}\nabla)\nabla\Phi^*, \quad w \equiv \frac{\partial\Phi}{\partial z} = L(\hat{z}\nabla)\frac{\partial\Phi^*}{\partial z},$$

from which we obtain

$$\hat{u}^* \equiv \nabla\hat{\Phi}^*, \quad \hat{w}^* \equiv \left(\frac{\partial\Phi^*}{\partial z} \right)_{z=\hat{z}}, \quad (42a, b)$$

where $\hat{\Phi}^* \equiv (\Phi^*)_{z=\hat{z}}$. Furthermore, by inserting (41) in (1) we find that Φ^* satisfies the Laplace equation, and that we can apply the Laplace operator successively to replace horizontal by vertical differentiations to obtain

$$\nabla^{2m}\Phi^* = (-1)^m \frac{\partial^{2m}\Phi^*}{\partial z^{2m}}. \quad (43)$$

The next step is to utilize the kinematic bottom condition (40), which defines a high-order relationship between \hat{u}^* and \hat{w}^* . We insert (42a, b) and (43) in (40) and obtain

$$\left(\frac{\partial\Phi^*}{\partial z} + \frac{4\lambda^2}{9} \frac{\partial^3\Phi^*}{\partial z^3} + \frac{\lambda^4}{63} \frac{\partial^5\Phi^*}{\partial z^5} - \lambda \frac{\partial^2\Phi^*}{\partial z^2} - \frac{\lambda^3}{9} \frac{\partial^4\Phi^*}{\partial z^4} - \frac{\lambda^5}{945} \frac{\partial^6\Phi^*}{\partial z^6} \right)_{z=\hat{z}} = 0. \quad (44)$$

Now we look for solutions to this equation of the form

$$\Phi^*(x, y, z, t) = \sum_{n=0}^N (z+h)^n \Phi_n(x, y, t), \quad (45a)$$

which means that

$$\frac{\partial^m\Phi^*}{\partial z^m} = \sum_{n=m}^N \Phi_n \frac{n!}{(n-m)!} (z+h)^{n-m}. \quad (45b)$$

By inserting (45b) in (44), and requiring that this equation is satisfied for all values of \hat{z} , we find that only even integer numbers from 0 to 10 are acceptable values for n and

that (44) is satisfied exactly for any choice of the remaining six coefficients $\phi_0, \phi_2, \phi_4, \phi_6, \phi_8, \phi_{10}$. To determine these six coefficients, we first use (42b) and (43) to establish expressions for $\hat{w}^*, \nabla^2 \hat{w}^*, \nabla^4 \hat{w}^*$ and $\hat{\Phi}^*, \nabla^2 \hat{\Phi}^*, \nabla^4 \hat{\Phi}^*$ in terms of vertical derivatives of the pseudo potential, insert (45b) and solve the resulting linear algebraic system to obtain

$$\phi_0 = \left(\frac{3840 - 975 \lambda^2 \nabla^2 + 20 \lambda^4 \nabla^4}{3840} \right) \hat{\Phi}^* - \left(\frac{2895 \lambda - 185 \lambda^3 \nabla^2 + \lambda^5 \nabla^4}{3840} \right) \hat{w}^*, \quad (46a)$$

$$\phi_2 = \left(\frac{561 \lambda \nabla^2 - 18 \lambda^3 \nabla^4}{768 \lambda} \right) \hat{\Phi}^* + \left(\frac{945 - 141 \lambda^2 \nabla^2 + \lambda^4 \nabla^4}{768 \lambda} \right) \hat{w}^*, \quad (46b)$$

$$\phi_4 = - \left(\frac{315 \lambda \nabla^2 - 16 \lambda^3 \nabla^4}{384 \lambda^3} \right) \hat{\Phi}^* - \left(\frac{315 - 105 \lambda^2 \nabla^2 + \lambda^4 \nabla^4}{384 \lambda^3} \right) \hat{w}^*, \quad (46c)$$

$$\phi_6 = \left(\frac{189 \lambda \nabla^2 - 14 \lambda^3 \nabla^4}{384 \lambda^5} \right) \hat{\Phi}^* + \left(\frac{189 - 77 \lambda^2 \nabla^2 + \lambda^4 \nabla^4}{384 \lambda^5} \right) \hat{w}^*, \quad (46d)$$

$$\phi_8 = - \left(\frac{135 \lambda \nabla^2 - 12 \lambda^3 \nabla^4}{768 \lambda^7} \right) \hat{\Phi}^* - \left(\frac{135 - 57 \lambda^2 \nabla^2 + \lambda^4 \nabla^4}{768 \lambda^7} \right) \hat{w}^*, \quad (46e)$$

$$\phi_{10} = \left(\frac{105 \lambda \nabla^2 - 10 \lambda^3 \nabla^4}{3840 \lambda^9} \right) \hat{\Phi}^* + \left(\frac{105 - 45 \lambda^2 \nabla^2 + \lambda^4 \nabla^4}{3840 \lambda^9} \right) \hat{w}^*, \quad (46f)$$

where $\lambda = h + \hat{z}$. In combination with (45a) this defines the pseudo-potential in terms of fourth-order spatial derivatives and tenth-order powers of the vertical coordinate.

The remaining problem is to transform the pseudo-velocity potential into a physical velocity potential. We shall make this transformation in two ways, resulting in slightly different results.

A. Transformation using a modified L-operator

The most obvious transformation is based on (41), where the L-operator is defined by (32) with (35a–d) for the case of $N=2$. Again, we apply the Laplace operator successively to replace horizontal by vertical differentiations, by which (41) is modified to

$$\Phi = \left(1 - \frac{\hat{z}^2}{18} \frac{\partial^2}{\partial z^2} + \frac{\hat{z}^4}{504} \frac{\partial^4}{\partial z^4} - \frac{\hat{z}^6}{15120} \frac{\partial^6}{\partial z^6} + \frac{\hat{z}^8}{362880} \frac{\partial^8}{\partial z^8} \right) \Phi^*. \quad (47)$$

Next, we insert (45a) in (47) and obtain

$$\Phi(x, y, z, t) = \phi_0 + \gamma_2 \phi_2 + \gamma_4 \phi_4 + \gamma_6 \phi_6 + \gamma_8 \phi_8 + \gamma_{10} \phi_{10}, \quad (48)$$

where

$$\gamma_2 = \left(\zeta^2 - \frac{1}{9} \hat{z}^2 \right), \quad (49a)$$

$$\gamma_4 = \left(\zeta^4 - \frac{2}{3} \hat{z}^2 \zeta^2 + \frac{1}{21} \hat{z}^4 \right), \quad (49b)$$

$$\gamma_6 = \left(\zeta^6 - \frac{5}{3} \hat{z}^2 \zeta^4 + \frac{5}{7} \hat{z}^4 \zeta^2 - \frac{1}{21} \hat{z}^6 \right), \quad (49c)$$

$$\gamma_8 = \left(\zeta^8 - \frac{28}{9} \hat{z}^2 \zeta^6 + \frac{10}{3} \hat{z}^4 \zeta^4 - \frac{4}{3} \hat{z}^6 \zeta^2 + \frac{1}{9} \hat{z}^8 \right), \quad (49d)$$

$$\gamma_{10} = \left(\zeta^{10} - 5 \hat{z}^2 \zeta^8 + 10 \hat{z}^4 \zeta^6 - 10 \hat{z}^6 \zeta^4 + 5 \hat{z}^8 \zeta^2 \right), \quad (49e)$$

with $\zeta \equiv z + h$, and where $\phi_0, \phi_2, \phi_4, \phi_6, \phi_8, \phi_{10}$ are given by (46a–f).

B. Transformation involving a vertical shift

In the following, we provide an alternative transformation procedure with the objective of obtaining exactly the same dispersion relation as in §4.3. Note that for brevity we leave out the x , y and t arguments of the functions but keep the z -arguments for clarity. The starting point is (4a) given in terms of the velocity potential, i.e.

$$\Phi(z) = \cos((z - \hat{z})\nabla)\Phi(\hat{z}) + \frac{\sin((z - \hat{z})\nabla)}{\nabla}w(\hat{z}). \quad (50)$$

Now, we replace \hat{z} by $z + \hat{z}$, which modifies (50) to

$$\Phi(z) = \cos(\hat{z}\nabla)\Phi(z + \hat{z}) - \frac{\sin(\hat{z}\nabla)}{\nabla}w(z + \hat{z}). \quad (51)$$

Note that (51) involves the z -variation of Φ on both sides of the equation, and it describes a transformation including a vertical shift of \hat{z} .

The next step is to insert (41) in the right-hand side of (51). With the arguments of the cos-, sin- and L-operators now being identical, we can, according to (35e, f), write (51) as

$$\Phi(z) = \left(1 - \frac{4\hat{z}^2\nabla^2}{9} + \frac{\hat{z}^4\nabla^4}{63}\right)\Phi^*(z + \hat{z}) - \left(\hat{z} - \frac{\hat{z}^3\nabla^2}{9} + \frac{\hat{z}^5\nabla^4}{945}\right)w^*(z + \hat{z}). \quad (52)$$

This equation guarantees that the dispersion relation will be identical to the one from §4.3. To prove this statement, we differentiate (52) with x to obtain $u(z)$ and with z to obtain $w(z)$. At $z=0$, the resulting expressions for $u(0)$ and $w(0)$ in terms of $\mathbf{u}^*(\hat{z})$ and $w^*(\hat{z})$ are identical to the results obtained from (37a, b) and (39a–d), and in combination with the mutual kinematic bottom condition (40) this leads to identical dispersion relations.

The final step in the transformation procedure is to use the Laplace operator successively to replace horizontal by vertical differentiations, and by inserting (42b) and (43) in (52) we obtain

$$\Phi(z) = \left\{ \left(1 + \frac{4\hat{z}^2}{9}\frac{\partial^2}{\partial z^2} + \frac{\hat{z}^4}{63}\frac{\partial^4}{\partial z^4} - \hat{z}\frac{\partial}{\partial z} - \frac{\hat{z}^3}{9}\frac{\partial^3}{\partial z^3} - \frac{\hat{z}^5}{945}\frac{\partial^5}{\partial z^5}\right)\Phi^* \right\}_{z \rightarrow z + \hat{z}}. \quad (53)$$

This defines the new transformation from pseudo- to physical variables: we insert (45a) in (53), perform the vertical differentiations, and finally make a vertical shift from z to $z + \hat{z}$. The result is an expression for the physical velocity potential, which is identical to (48) with the only exception that the γ_{10} coefficient from (49e) is modified to

$$\tilde{\gamma}_{10} = \gamma_{10} - \hat{z}^{10}. \quad (54)$$

5.1. Accuracy of velocity profiles

The resulting velocity field can be expressed by

$$\mathbf{u}(x, y, z, t) \equiv \nabla\Phi = \sum_{n=0}^2 \alpha_{2n} \nabla^{2n} \hat{\mathbf{u}}^* + \sum_{n=0}^2 \alpha_{2n+1} \nabla^{2n+1} \hat{w}^*, \quad (55a)$$

$$w(x, y, z, t) \equiv \frac{\partial\Phi}{\partial z} = \sum_{n=0}^2 \beta_{2n} \nabla^{2n} \hat{w}^* + \sum_{n=0}^2 \beta_{2n+1} \nabla^{2n+1} \hat{\mathbf{u}}^*, \quad (55b)$$

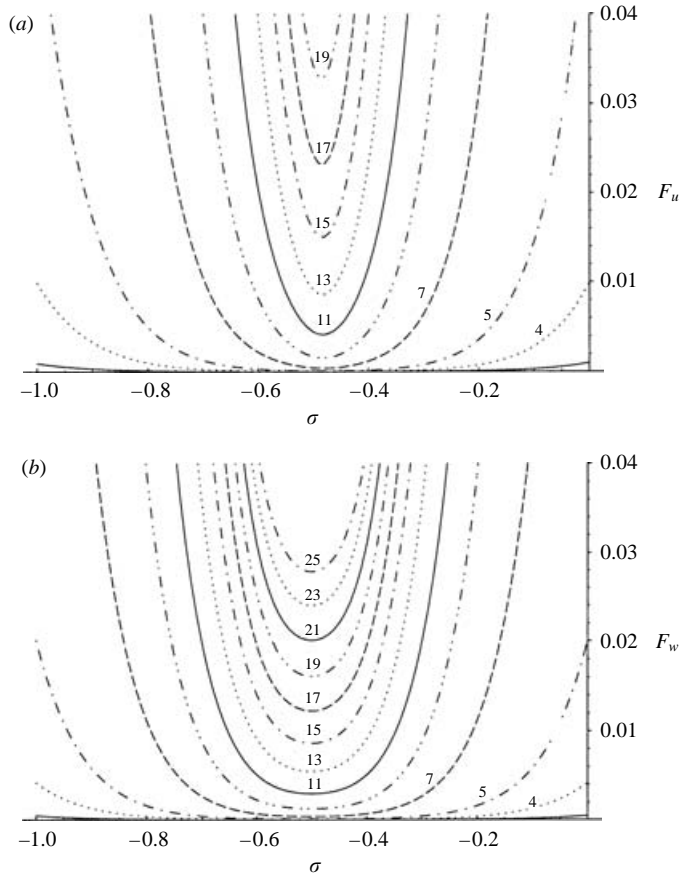


FIGURE 11. (a) The error F_u and (b) F_w as functions of σ for discrete values of kh . Second-order ($N = 2$) velocity profile based on § 5.2, i.e. (48) with (49a–e) and (46a–f).

which involves algebraic but rather lengthy expressions for α_j, β_j with $j = 0, 1, 2, 3, 4, 5$. Note that (55a, b) involve 12 different velocity coefficients, in contrast to (37a, b) which (with $N = 2$) involve only six different coefficients. The order of the spatial derivatives is, however, the same in (37a, b) and (55a, b).

It turns out that, whether we use transformation A leading to (49a–e), or transformation B replacing (49e) by (54), it makes no difference to the vertical velocity $w(z)$, while the horizontal velocity $u(z)$ is changed accordingly. In both cases, however, the formal accuracy of $u(z)/u(0)$ is $O(k^{10}h^{10})$ compared to Stokes target solution, while it is $O(k^8 h^8)$ for the vertical velocity ratio.

Figure 11(a, b) shows the computed errors F_u and F_w defined by (19a, b) for the case of transformation A, and the optimal choice of σ is found to be -0.48 and -0.500 , respectively. For the case of transformation B, figure 11(a) is slightly modified as the optimal choice of σ becomes -0.500 , but the overall accuracies are very similar to figure 11(a).

The last column in table 5 summarizes the kh -values corresponding to 2% errors in u and w for a range of σ -values using transformation A. For $\sigma = -0.49$ the 2% errors are reached at $kh = (16.24, 20.96)$. This is a 30% increase for F_u and a 67% increase for F_w in comparison with the method from § 4.3, and it is superior to any

of the other $N = 2$ methods. Another attraction is the relatively high accuracy which can be achieved for the case of $\sigma = 0$, for which the 2% error limits in (F_u, F_w) are reached at $kh = (4.38, 5.0)$. These values are outstanding compared to other methods based on $\sigma = 0$.

The accuracy of the linear dispersion relation, corresponding to the two different transformations will be discussed in § 6.

6. Involving the linearized boundary conditions at the still-wates level

Throughout §§ 3 to 5 we have ignored the influence of the dynamic and kinematic boundary conditions at the surface in order to focus on the accuracy and convergence of various power series solutions satisfying the Laplace equation and the kinematic bottom condition. With this objective we have analysed the shape of the velocity profiles scaled relative to the horizontal and vertical velocities at still-wates level ($z = 0$), but until now we have not considered the accuracy of these scaling velocities compared to linear theory. Consequently, §§ 3 to 5 provide *necessary but not sufficient* measures of the range of applicability of a certain formulation.

To establish the linear accuracy in an absolute sense we need to involve the linearized surface boundary conditions at $z = 0$, given by (15a,b):

$$\frac{\partial \mathbf{u}_0}{\partial t} + g \nabla \eta = 0, \quad \frac{\partial \eta}{\partial t} - w_0 = 0.$$

A linear Fourier analysis of these equations combined with the velocity formulations from §§ 3 to 5, leads to the determination of the imbedded linear dispersion relation and the amplitude of the horizontal still-water velocity expressed in terms of the amplitude of the surface elevation.

We illustrate the procedure for the methods described in § 3.1. The starting point is a harmonic solution of the form

$$\eta(x, t) = a e^{i\theta}, \quad \hat{u}(x, t) = B_1 e^{i\theta}, \quad \theta = \omega t - kx,$$

and by the use of (17a,b) we find

$$u_0(x, t) = B_1 \Lambda_u e^{i\theta}, \quad w_0(x, t) = B_1 \Lambda_w i e^{i\theta},$$

where Λ_u, Λ_w depend upon the order of the expansion used in (17a,b) and are functions of kh and σ . Inserting this into (15a,b) leads to solutions for the dispersion relation and the velocity coefficient,

$$\frac{\omega^2}{ghk^2} = \frac{\Lambda_w}{kh \Lambda_u}, \quad B_1 = \frac{a\omega}{\Lambda_w},$$

from which we obtain

$$u_0(x, t) = \left(\frac{a\omega \Lambda_u}{\Lambda_w} \right) e^{i\theta} = \left(\frac{gka}{\omega} \right) e^{i\theta}, \quad w_0(x, t) = a\omega i e^{i\theta}.$$

Hence we can conclude that the accuracy of the SWL velocities is determined entirely by the linear dispersion relation for the relevant set of Boussinesq equations. Similar conclusions can be made on the basis of the other velocity formulations in §§ 3 to 5.

In figure 12, we present the accuracy of the linear dispersion relation as the squared ratio of the celerity to Stokes linear target solution, and we plot this ratio as a

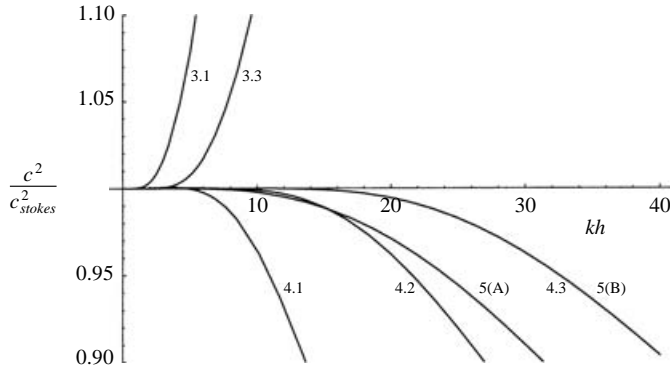


FIGURE 12. The square of the linear phase celerity divided by the target solution. All formulations expanded to $N=2$ (i.e. including fifth derivatives). Curve 3.1: §3.1 with $\sigma = -0.672$; 3.3: §3.3; 4.1: §4.1 with $\sigma = -0.5$; 4.2: §4.2 with $\sigma = -0.5$; 4.3: §4.3 with $\sigma = -0.5$; 5(A): §5, transformation A, with $\sigma = -0.49$; 5(B): §5 (transformation B) with $\sigma = -0.5$ (identical to 4.3).

function of kh . Only the methods of order 2 (i.e. with fifth derivatives) from §§3.1, 3.3, 4.1, 4.2, 4.3, and 5 are included. The method from §3.3 corresponds to a Padé (4,4) expansion of the target solution, while the other methods contain fractions of eighth-order polynomials divided by tenth-order polynomials without being exactly a Padé (8,10) expansion. We notice that the new method from §5 with transformation A has a dispersion relation which is slightly more accurate than the one from §4.2. When the method from §5 is combined with transformation B, it has exactly the same dispersion relation as the one from §4.3, and both methods have errors in c^2 of less than 2% for kh as high as 25 for $\sigma = -0.5$.

7. Involving the exact boundary conditions at the free surface

To obtain the full picture of the accuracy of a certain method, it must be tested on the fully nonlinear water wave problem. This involves the exact dynamic and kinematic boundary conditions at the free surface. In the following we present a spectral solution for steady nonlinear waves on a constant depth in one horizontal dimension, and the analysis is limited to the two methods from §§4.3 and 5, which have been shown to be superior to other alternatives. For both methods it is advantageous to apply a two-step approach for nonlinear waves. The first step describes the region between the moving free surface and the still-water datum (SWL) by using (4a, b) with $\hat{z}=0$, which leads to

$$u(x, z) = \left(1 - \frac{z^2 \nabla^2}{2} + \frac{z^4 \nabla^4}{24}\right) u_0 + \left(z \nabla - \frac{z^3 \nabla^3}{6} + \frac{z^5 \nabla^5}{120}\right) w_0, \tag{56a}$$

$$w(x, z) = \left(1 - \frac{z^2 \nabla^2}{2} + \frac{z^4 \nabla^4}{24}\right) w_0 - \left(z \nabla - \frac{z^3 \nabla^3}{6} + \frac{z^5 \nabla^5}{120}\right) u_0, \tag{56b}$$

where $0 \leq z \leq \eta$. The second step describes the region from the SWL to the sea bottom, where the method from §4.3 is based on (37a, b) combined with (40), while the method from §5 (case B) is based on (53) and (45a) combined with (46a-f). In both methods the velocities at the SWL are connected to the pseudo-velocities at

$z = \hat{z}$ through (36a, b) with $z = 0$, which leads to

$$\mathbf{u}_0 = \left(1 - \frac{4\hat{z}^2\nabla^2}{9} + \frac{\hat{z}^4\nabla^4}{63}\right) \hat{\mathbf{u}}^* - \left(\hat{z}\nabla - \frac{\hat{z}^3\nabla^3}{9} + \frac{\hat{z}^5\nabla^5}{945}\right) \hat{w}^*, \quad (57a)$$

$$w_0 = \left(1 - \frac{4\hat{z}^2\nabla^2}{9} + \frac{\hat{z}^4\nabla^4}{63}\right) \hat{w}^* + \left(\hat{z}\nabla - \frac{\hat{z}^3\nabla^3}{9} + \frac{\hat{z}^5\nabla^5}{945}\right) \hat{\mathbf{u}}^*. \quad (57b)$$

Furthermore the two methods share the same formulation (40) of the kinematic bottom condition. Now (56a, b) with $z = \eta$ defines the connection between the surface velocities $\tilde{\mathbf{u}}, \tilde{w}$ and the SWL velocities \mathbf{u}_0, w_0 while (57a, b) defines the connection between \mathbf{u}_0, w_0 and $\hat{\mathbf{u}}^*, \hat{w}^*$.

For the case of steady nonlinear waves, we can use the transformation

$$\frac{\partial}{\partial t} = -c \frac{\partial}{\partial x},$$

where c is the constant wave celerity. In this case, the kinematic and dynamic free-surface conditions simplify to

$$-\tilde{w} + (\tilde{u} - c)\eta_x = 0, \quad -c\tilde{u} + g\eta + \frac{\tilde{u}^2}{2} + \frac{\tilde{w}^2}{2} = R, \quad (58a, b)$$

where R is the Bernoulli constant. The dynamic pressure (in excess of the hydrostatic part) can be determined by

$$\frac{p^+(x, z)}{\rho} = cu(x, z) - \frac{1}{2}(u(x, z)^2 + w(x, z)^2). \quad (59)$$

We look for spectral solutions to the problem, and expand the surface elevation and the velocity variables at \hat{z} in terms of the Fourier series

$$\eta(x) = \sum_{j=1}^M A_j \cos(jkx), \quad (60a)$$

$$\hat{\mathbf{u}}^*(x) = \sum_{j=1}^M B_j \cos(jkx), \quad \hat{w}^*(x) = \sum_{j=1}^M C_j \sin(jkx). \quad (60b, c)$$

A connection between the C_j and the B_j coefficients is determined by using the kinematic bottom condition (40). Given the three inputs H (wave height), h (water depth), and L (wavelength), and assuming zero mean Eulerian velocity, there are two kinematic constraints,

$$H = \eta(0) - \eta\left(\frac{L}{2}\right), \quad c = \frac{L}{T},$$

plus the free-surface boundary conditions (58a, b). The dynamic surface condition is applied at $M + 1$ equally spaced points from the wave trough to the wave crest, while the kinematic condition is applied at M staggered points (mid-way between the others). This gives $2M + 3$ nonlinear equations for the unknowns T (wave period), c , R and the coefficients A_j and B_j . The system is readily solved using Newton's method with linear theory as the initial conditions.

To establish a reference solution (similar to the stream function solution presented by e.g. Fenton 1988) we use the above technique and solve the fully dispersive problem

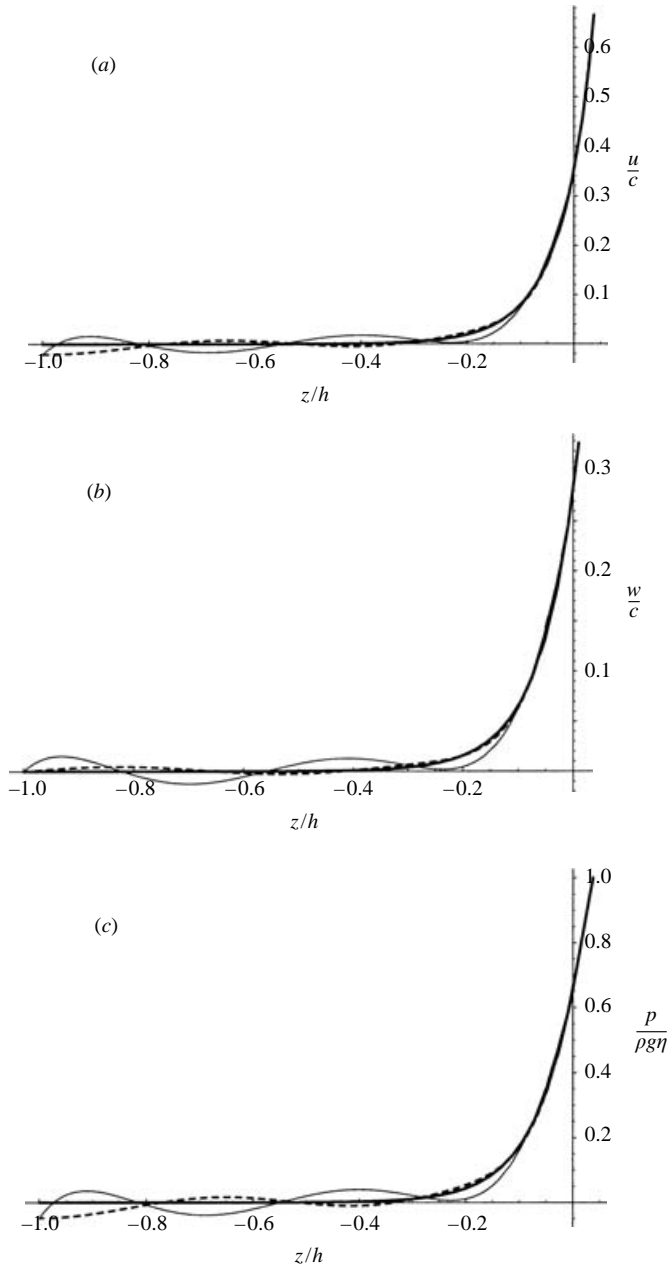


FIGURE 13. Vertical distribution of (a) the horizontal velocity under the wave crest, (b) the vertical velocity at $x/L = 0.15$ and (c) the dynamic pressure under the wave crest. Steady deep water wave with $kh = 14$ and $H/L = 0.13$. Full line: Exact stream function solution. Dashed line: Method from Section 5(A). Thin full line: Method from Section 4.3.

by replacing (56a, b), (57a, b) and (40) by

$$u(x, z) = \sum_{j=1}^M B_j \frac{\cosh(jk(z + h))}{\cosh(jkh)} \cos(jkx), \tag{61a}$$

kh	F_u	F_w	F_{p^+}
(a) 6	0.00440	0.00356	0.00510
9	0.01034	0.00967	0.01220
12	0.01724	0.01681	0.02052
16	0.02635	0.02545	0.03155
(b) 6	0.00165	0.00042	0.00200
9	0.00498	0.00189	0.00605
12	0.01025	0.00429	0.01246
16	0.01964	0.00775	0.02403

TABLE 6. Depth-integrated errors for u , w , p^+ for nonlinear steady waves. $H/L = 0.13$. (a) Method from § 4.3 and (b) method from § 5 with $\sigma = -0.5$.

$$w(x, z) = \sum_{j=1}^M B_j \frac{\sinh(jk(z+h))}{\cosh(jkh)} \sin(jkx). \quad (61b)$$

As an example which stretches the two Boussinesq methods to their limits, we consider the strongly nonlinear case of $H/L=0.13$ and $kh=14$. The vertical distributions of the horizontal velocity (at the wave crest) and of the vertical velocity (at the section where it is maximum) are shown in figure 13(a, b), while the dynamic pressure distribution under the wave crest is shown in figure 13(c). The reference solutions (thick lines) are compared to the two Boussinesq methods from § 4.3 (dashed lines) and § 5 (thin lines), both applied with $\sigma = -0.5$. We note that above the still-water level the two Boussinesq methods are identical and in excellent agreement with the reference solution. Below the still-water level, the method from § 5 is generally more accurate than the one from § 4.3.

To quantify the accuracy we use the error measures from (19a, b) with the modification that the integration is continued up to the free surface. A similar error measure is determined for the dynamic pressure given by (59). The errors for the pressure and the horizontal velocities are determined under the wave crest, while the errors for the vertical velocity are determined at the section $x/L = 0.15$. The results are shown in tables 6(a) and 6(b) for the methods from §§ 4.3 and 5, respectively.

8. Summary and conclusions

The objective of this paper has been to discuss and analyse the accuracy of various velocity formulations for water waves in the framework of Boussinesq theory. Throughout the paper, we have focused on the problem of finding truncated series solutions to the Laplace equation with a kinematic condition at the horizontal sea bed. The convergence and accuracy of the resulting expressions has been analysed and compared with the target cosh- and sinh-functions from linear wave theory. Generally, we have investigated the various formulations in a first-order form (with third-order derivatives), a second-order form (with fifth-order derivatives) and a fourth-order form (with ninth-order derivatives).

First, in § 3.1, we have considered series expansions in terms of the horizontal velocity variable at an arbitrary z -level, which can be varied from the sea bottom to the still-water datum. Second, in § 3.2, we have considered expansions in terms of the depth-averaged velocity. Third, in § 3.3, we have analysed the use of a horizontal pseudo-velocity determined by interpolation between velocities at two arbitrary z -levels.

$N = 2$ methods	Based on $\sigma = 0$	Based on σ^{uw}	σ^{uw}
§ 3.1	0.88, 1.15	4.75, 5.39	-0.672
§ 3.2	-	1.77, 1.98	-
§ 3.3	-	5.13, 5.58	-
§ 4.1	1.73, 2.04	6.14, 6.84	-0.533
§ 4.2	2.01, 2.02	6.61, 6.62	-0.494
§ 4.3	2.01, 2.02	12.59, 12.48	-0.489
§ 5	4.38, 5.00	16.22, 20.99	-0.490

TABLE 7. Limiting wavenumbers kh_u, kh_w for which F_u, F_w exceed 2%.

The different options covered in § 3 include most of the conventional formulations from the literature, and we can conclude that many of these have a relatively poor accuracy and applicability.

The reason for this rather disappointing performance is the polynomial representation of the tan-operator, which appears in the kinematic bottom condition when the vertical velocity variable is explicitly expressed in terms of the horizontal one. Due to the inherent pole of this operator, polynomial representations result in a limited convergence radius, which makes it difficult to improve accuracy even with high-order formulations. However, by avoiding the explicit elimination of the vertical particle velocity at the expansion level and keeping it as one of the unknowns, the tan-operator can be represented by a rational function of two polynomials and this effectively makes the convergence radius grow with the number of terms included.

Three such methods (derived recently by Madsen *et al.* 2002*b*) are investigated in §§ 4.1, 4.2 and 4.3, and they all have unlimited convergence radius. Of these, the method in § 4.3 is by far the most accurate as it incorporates Padé approximants in the kinematic bottom condition as well as at $z = 0$. As a consequence, the accuracy is significantly improved and with fifth-order derivatives ($N = 2$) this method is almost as accurate as the one from § 4.1 with ninth-order derivatives ($N = 4$).

Further improvement of accuracy is obtained in § 5, where a new formulation is derived as an extension to the method from § 4.3. This method doubles the power of the vertical coordinate without increasing the order of horizontal derivatives, and the resulting velocity profiles, with up to fifth derivatives in the horizontal and with polynomial powers in z up to ten, are highly accurate.

In table 7, we summarize the accuracy of the different methods from §§ 3 to 5 for the case of $N = 2$ (i.e. including fifth derivatives). The second and third columns show the limiting wavenumbers kh for which F_u, F_w exceed 2% using $\sigma = 0$ and $\sigma = \sigma^{uw}$ respectively. The values of σ^{uw} are given in the last column of table 7. We note that these values are a compromise between the optimal σ^u determined on the basis of the u -profiles and σ^w determined from the w -profiles. These optimal levels are not necessarily identical as show below:

$$\begin{aligned} \sigma_{3,1}^u &= -0.672, \sigma_{3,1}^w = -0.717; & \sigma_{4,1}^u &= -0.533, \sigma_{4,1}^w = -0.484; & \sigma_{4,2}^u &= -0.494, \\ \sigma_{4,2}^w &= -0.494; & \sigma_{4,3}^u &= -0.489, \sigma_{4,3}^w = -0.489; & \sigma_5^u &= -0.480, \sigma_5^w = -0.500. \end{aligned}$$

In §§ 3 to 5, we have ignored the boundary conditions at the free surface in order to discuss the quality of the velocity profiles without involving the imbedded linear dispersion relation or nonlinear effects from the moving free surface. In § 6,

however, the accuracy of the linear dispersion corresponding to the different methods is summarized. On this basis and on the basis of table 7, it can be concluded that from a linear point of view the methods discussed in §§ 4.3 and 5 are superior.

In order to investigate to what extent the accuracy carries over to the case of nonlinear waves, we present a spectral solution for steady nonlinear waves in § 7. The vertical distribution of the horizontal velocity, the vertical velocity and the dynamic pressure is compared to a stream function solution. Based on a 2% error criterion, it is found that the methods from §§ 4.3 and 5 can be applied for highly nonlinear waves ($H/L=0.13$) up to $kh \approx 12$ and $kh \approx 16$, respectively. In shallow water the difficult part of the velocity profile is above the still-water level and in this region the two methods from §§ 4.3 and 5 are identical according to (56*a, b*). In Madsen *et al.* (2002*a*) we have previously demonstrated the accuracy of this approach to cover the case of highly nonlinear solitary waves.

It should be mentioned that throughout this paper we have assumed a constant depth in order to keep the analyses as simple as possible. However, except for the new method in § 5, all other methods have previously been extended and tested on a mildly sloping bottom. This aspect is beyond the scope of the present paper but readers are referred to e.g. Agnon *et al.* (1999) and Madsen *et al.* (2002*a, b*).

One reviewer has raised the question of to what extent the various theories presented in this paper should really be considered as Boussinesq theories? This is an interesting question as there is no doubt that most of today's state-of-the-art formulations are rather different and a lot more complicated than what was originally proposed by Boussinesq (1872).

First, an important difference is the fact that the parameter of non-linearity (ϵ) is no longer assumed to be small and of the same order as the dispersion parameter (μ^2). This change has made it possible to consider higher waves, and waves interacting with currents including Doppler shift (see e.g. Madsen & Schäffer 1998).

Second, a dramatic change has been the extension of the linear dispersion relation, which has made it possible to consider waves in deeper water and to extend the applicability in terms of $\mu(=kh)$ from approximately 0.5 to several times π (the traditional deep-water limit).

Third, there are differences with respect to the truncated velocity field: In line with Boussinesq (1872), most state-of-the-art formulations exactly satisfy zero vorticity but only approximately satisfy local continuity. However, we recommend the alternative to exactly satisfy local continuity but only approximately satisfy zero vorticity. And to complete the picture, the more advanced methods (described in §§ 4 and 5) satisfy neither local continuity nor zero vorticity exactly.

Fourth, there is the appearance of the governing equations: in all the methods described in § 3, the vertical velocity variable is eliminated and the resulting mass and momentum equations are given in terms of the surface elevation and a horizontal velocity variable. However, the methods described in §§ 4 and 5 are quite different as they maintain the vertical velocity variable as one of the unknowns and result in six (or more) coupled equations rather than the usual two.

So what do these different methods really have in common with the original Boussinesq approach? They all remove the vertical coordinate from the governing equations by using truncated power series expansions which replace vertical differentiation with horizontal differentiation and introduces relatively high powers (third order as a minimum) of the horizontal gradient operator into the governing equations. For this reason we have chosen to consider the variety of methods described in this paper to belong to the family of Boussinesq-type methods.

Finally, it should be mentioned that the present work can be considered in the broader context of approximation to irrotational flow, rather than just Boussinesq modelling of water waves. By using the techniques described in this paper, many irrotational flows (and axisymmetric flows) can be studied to high order taking out one dimension. We present this idea, which was proposed to us by Professor Howell Peregrine, but we do not pursue it further here, as it is beyond the scope of the present paper.

This work was partly financed by the Danish Technical Research Council (STVF grant no. 9801635). Inspiring discussions with Dr Hemming Schäffer and Mr Henrik Bredmose are also acknowledged.

REFERENCES

- AGNON, Y., MADSEN, P. A. & SCHÄFFER, H. A. 1999 A new approach to high order Boussinesq models. *J. Fluid Mech.* **399**, 319–333.
- BAKER, G. A. & GRAVES-MORRIS, P. 1981 Padé approximants. Part I: Basic theory. In *Encyclopedia of Mathematics and its Applications*, Vol 13. Addison Wesley.
- BENJAMIN, T. B., BONA, J. L. & MAHONY, J. J. 1972 Model equations for long waves in non-linear dispersive systems. *Phil. Trans. R. Soc. Lond. A* **272**, 47–78.
- BOUSSINESQ, J. 1872 Théorie des ondes et des remous qui se propagent le long d'un canal rectangulaire horizontal, en communiquant au liquide contenu dans ce canal des vitesses sensiblement pareilles de la surface au fond. *J. Math. Pures Appl.* (2) **17**, 55–108.
- CHEN, Y. & LIU, P. L.-F. 1995 Modified Boussinesq equations and associated parabolic models for water wave propagation. *J. Fluid Mech.* **288**, 351–381.
- DINGEMANS, M. 1973 Water waves over an uneven bottom; a discussion of long-wave equations. *Delft Hydraulics Rep. R729*, part 2.
- DINGEMANS, M. 1997 *Water Wave Propagation over Uneven Bottoms*. Advanced Series on Ocean Engineering, Vol 13, Parts 1, 2, World Scientific.
- FENTON, J. D. 1988 The numerical solution of steady water wave problems. *Comput. Geosci.* **14**, 357–368.
- GOBBI, M. F. & KIRBY, J. T. 1999 Wave evolution over submerged sills: Tests of a high-order Boussinesq model. *Coastal Engng* **37**, 57–96.
- GOBBI, M. F., KIRBY, J. T. & WEI, G. 2000 A fully nonlinear Boussinesq model for surface waves. Part 2. Extension to $O(kh)^4$. *J. Fluid Mech.* **405**, 181–210.
- HILDEBRAND, F. B. 1976 *Advanced calculus for Applications* (2nd Edn.), Prentice-Hall.
- KENNEDY, A. B., KIRBY, J. T. & GOBBI, M. F. 2002 Simplified higher order Boussinesq equations. 1: Linear simplifications. *Coastal Engng* **44**, 205–231.
- MADSEN, P. A., BINGHAM, H. B. & LIU, H. 2002(a) A new Boussinesq method for fully nonlinear waves from shallow to deep water. *J. Fluid Mech.* **462**, 1–30.
- MADSEN, P. A., BINGHAM, H. B. & SCHÄFFER, H. A. 2002(b) Boussinesq-type formulations for fully nonlinear and extremely dispersive water waves: derivation and analysis. *Proc. R. Soc. Lond. A* (to appear).
- MADSEN, O. S. & MEL, C. C. 1969 The transformation of a solitary wave over an uneven bottom. *J. Fluid Mech.* **39**, 781–791.
- MADSEN, P. A. & SCHÄFFER, H. A. 1998 Higher order Boussinesq-type equations for surface gravity waves – Derivation and analysis. *Phil. Trans. R. Soc. Lond. A* **356**, 1–59.
- MADSEN, P. A. & SCHÄFFER, H. A. 1999 A review of Boussinesq-type equations for gravity waves. In *Advances in Coastal and Ocean Engineering*, Vol. 5 (ed. P. Liu), pp. 1–95, World Scientific.
- MADSEN, P. A., MURRAY, R. & SØRENSEN, O. R. 1991 A new form of the Boussinesq equations with improved linear dispersion characteristics. Part 1. *Coastal Engng* **15**, 371–388.
- MEL, C. C. 1983 *The Applied Dynamics of Ocean Surface Waves*. John Wiley.

- MEI, C. C. & LEMÉHAUTÉ, B. 1966 Note on the equations of long waves over an uneven bottom. *J. Geophys. Res.* **71**, 393–400.
- NWOGU, O. 1993 Alternative form of Boussinesq equations for nearshore wave propagation. *J. Waterways, Port, Coastal, Ocean Engng ASCE* **119**, 618–638.
- PEREGRINE, D. H. 1967 Long waves on a beach. *J. Fluid Mech.* **27**, 815–827.
- PRESS, W. H., TEUKOLSKY, S. A., VETTERLING, W. T. & FLANNERY, B. P. 1992 *Numerical Recipes in Fortran 77*, Vol 1. Cambridge University Press.
- SERRE, P. F. 1953 Contribution à l'étude des écoulements permanents et variables dans les canaux. *La Houille Blanche* 374–388; 830–872.
- SU, C. H. & GARDNER, C. S. 1969 Korteweg-de Vries equation and generalizations. III. Derivation of the Korteweg-de Vries equation and Burgers equation. *J. Math. Phys.* **10**, 536–539.
- WEI, G., KIRBY, J. T., GRILLI, S. T. & SUBRAMANYA, R. 1995 A fully nonlinear Boussinesq model for surface waves. Part 1. Highly nonlinear unsteady waves. *J. Fluid Mech.* **294**, 71–92.
- WHITHAM, G. B. 1974 *Linear and Non-linear Waves*. Wiley-Interscience.
- WITTING, J. M. 1984 A unified model for the evolution of nonlinear water waves. *J. Comput. Phys.* **56**, 203–236.
- WU, T. Y. 1999 Modelling nonlinear dispersive water waves. *J. Engng Mech.* **125**, 747–755.
- WU, T. Y. 2001 A unified theory for modelling water waves. *Adv. Appl. Mech.* **37**, 1–88.